Supplementary Information

A climate risk index for marine life

Daniel G. Boyce, Derek P. Tittensor, Cristina Garilao, Stephanie Henson, Kristin Kaschner, Kathleen Kesner-Reyes, Alex Pigot, Rodolfo B. Reyes Jr. Gabriel Reygondeau, Kathryn E. Schleit, Nancy Shackell, Patricia Sorongon-Yap, Boris Worm

Contents

Overview **2**

1. Defining climate vulnerability: data, indices, and dimensions **5**

2. Data compilation **7**

Overview 7
Species native geographic distribution *7*
Species traits *8*
Environmental conditions *10*
Climate projections *11*

3. Calculation of the indices **11**

Overview 11

Notes on standardization: reference values and scaling 11

Climate sensitivity indices 13
Overview *13*
Thermal safety margins *13*
Conservation status of species *14*
Cumulative impacts *16*
Vertical habitat variability and use *17*

Climate exposure indices 19
Overview *19*
Projected time of climate emergence *19*
Projected ecosystem disruption *21*
Projected loss of suitable thermal habitat *23*
Projected climate velocity *25*

Adaptivity to climate indices 26
Overview *26*
Geographic range extent *26*
Geographic habitat fragmentation *28*
Thermal habitat variability and use *30*
Maximum body length *32*

4. Calculating climate vulnerability **34**

Species across their geographic distributions 34

Species 37

5. Calculating climate risk 38

6. Quality control and sensitivity analyses 43

Criteria for species inclusion 43

Thresholds of acceptable index missingness 44

Thresholds of acceptable data spatial missingness 45

The sensitivity of the analyses to the transformation functions 46

Missing data 49

Imputation of body lengths *49*

Gap-filling of Red List statuses *50*

Defining species native geographic distribution 50

Collinearity of climate indices 52

Vulnerability across the ecosystem 52

Supplementary figures 55

References 58

Overview

Climate change vulnerability emerged as a research field in the 1990s in response to climate change, natural hazard and disaster planning, and endangered species research. Initial climate change vulnerability research was firmly focused on the vulnerability of terrestrial systems, including primarily humans. The field has expanded from this beginning, and climate change vulnerability assessments (CCVAs) are now widely viewed as a critical component of climate-smart management of species and ecosystems and quantifying climate change impacts[1–3]. CCVAs seek to address several critical questions related to the effects of climate on species and ecosystems, namely, *which* are most vulnerable, *where* they are most vulnerable *when* they become vulnerable, and *why* they are vulnerable. CCVAs can also identify gaps in data and information needed to understand climate change impacts on species and ecosystems. To this end, over 800 peer-reviewed CCVAs have been developed to evaluate the vulnerability of species, communities and ecosystems across different scales and systems, using various approaches (*e.g.* trait-based, correlative, mechanistic modelled, theoretical)[*e.g.* 4–6]. This interest has led to a broad acceptance of what features define vulnerability. Following an early IPCC definition[7] and subsequent broad adoption[4–6,8–10], species' climate vulnerability has been defined by three dimensions: their sensitivity, exposure, and adaptive capacity (adaptivity) to climate change. Sensitivity refers to the propensity for a species to be adversely affected by its exposure to climate change. Exposure refers to the extent to which species will be subjected to hazardous climate changes, including the magnitude of the effects. Adaptivity refers to the potential of species to adapt to any adverse exposure to climate change. These dimensions have close analogies in other disciplines, including

community ecology and dynamic complex systems theory[11–13]. For example, sensitivity is analogous to the ecological concept of resistance, exposure is analogous to reactivity, and adaptivity is analogous to resilience[14–16]. Thus, the dimensions that define climate vulnerability are rooted in ecological theory.

Despite the tremendous interest in assessing climate vulnerability and the hundreds of vulnerability analyses[4,5], these methods have not been consistently applied across species, locations, geographic scales, or time. Further, climate vulnerability assessments are rarely applied in marine management settings[6], such as fisheries, species at risk, or spatial planning. Reviews have reported that vulnerability studies often incorporate expert opinions, such as subjective species rankings, rather than quantitative approaches (objective data and reproducible methods), have been locally or regionally focused[4–6], and infrequently incorporate all dimensions that are accepted to define vulnerability, including sensitivity, exposure, and adaptivity. For instance, of 743 climate change vulnerability studies, De los Rios *et al.* [5] reported that only 11% had considered all three dimensions that collectively define vulnerability, and a review by Pacifici *et al.* [6] reported that only 4% of assessments were global. Notably, CCVAs report vulnerability as relative scores and rankings, which may have hindered their uptake and application in management settings.

The climate change risk assessment (CCRA) described here integrates the knowledge accumulated in previous climate change studies and CCVAs to develop a unified framework for assessing both relative climate vulnerability and absolute climate risk that fills several of these existing gaps. It enables the vulnerability and risk of marine species to be assessed at all locations across their geographic distributions in a spatially explicit, quantitative, reproducible, consistent, and standardized manner, can be applied at scales from local to global, can incorporate new information as it becomes available, and is transparent, and evaluates the statistical uncertainty of estimated vulnerability and risk. Perhaps most critically, the framework provides a robust method for translating relative vulnerability scores and rankings into absolute risk categories for species and ecosystems to aid the management and conservation of marine ecosystems under climate change. The CCRA consists of the following overarching design principles:

1. **Generalized and adaptable:** The information used to define vulnerability and risk represent generalized responses of species to climate change operating consistently across species with varying taxonomies and life histories. The approach is designed to be minimal-realistic and a starting platform upon which to build. Here, we developed an approach with the understanding that its utility depends on its goals and objectives, which may differ across users. A global minimal-realistic CCRA may be appropriate for those seeking a broad overview of vulnerability, but additional climate information may be required for those seeking to evaluate the vulnerability of fisheries, for instance. It is also anticipated that new climate-relevant information will become increasingly available and the framework is developed to flexibly incorporate this information should it be deemed relevant.
2. **Quantitative and comprehensive:** Several existing CCVAs have been developed using semi-quantitative rankings based on expert opinion[*e.g.* 3,10]. These approaches are sensible but are also difficult to reproduce and labour-intensive, particularly at large scales. This limits their reproducibility, making it

challenging to monitor vulnerability in a standardized manner over time. This study prioritizes the use of measurable, quantitative information sources to facilitate the reproducibility of the assessment. De los Rios *et al.* [5] reported that only 11% of vulnerability assessments had included all three dimensions widely accepted to define it (sensitivity, adaptivity, exposure), and those that do often contain only a single index to define each dimension. This study represents and integrates all three vulnerability dimensions and comprehensively uses multiple indices to define each dimension robustly. The framework also defines the indices using a comprehensive range of approaches, including correlative, trait-based, and mechanistic, across various biological organization levels, from species to ecosystems and incorporating past, present, and future climate data.

3. **Globally and taxonomically standardized and scalable:** Species vulnerability assessments are predominantly conducted at local or regional scales[6], making it difficult to interpret them globally, limiting their interpretability and use. We standardize vulnerability estimates using immutable scaling factors and statistical transformations to interpret the vulnerability scores for individual species and/or locations on a standardized scale across all sites and species. This scalability ensures that the framework can be applied at varying spatial (*e.g.* local, regional, global) and taxonomic (*e.g.* species, ecosystems) scales, thus accommodating different goals and objectives. The vulnerability scores' interpretation is preserved through this scalability when they are downscaled from coarser global resolutions to higher-resolutions and more scale-appropriate data layers used (*e.g.* regional climate models).
4. **Practical, transparent and parsimonious:** The framework uses robust yet broadly interpretable methods to encourage its ongoing use and development. To increase transparency, the framework prioritized using publicly available, peer-reviewed data and integrated it using the most parsimonious methods. To this end, the framework maximizes the information related to species' climate vulnerability and risk while minimizing data volume and complexity. As some species or regions are data-limited, sensitivity analyses were performed to determine the acceptable data completeness thresholds.

With these overarching design principles in mind, climate vulnerability and risk were evaluated for each species (taxonomically) at all locations across their native geographic distributions (spatial) and superimposed to explore ecosystem patterns; the main steps in this process were:

1. **Identification of indices of climate sensitivity, exposure and adaptivity.**
2. **Data compilation.**
3. **Calculation of climate indices.**
4. **Calculation of climate vulnerability.**
5. **Calculation of climate risk**
6. **Quality control, sensitivity, and robustness analyses.**

The following text describes these steps and, as an illustrative example, assesses Shortfin mako's (*Isurus oxyrinchus*) climate vulnerability and risk under the IPCC's shared socioeconomic pathway (SSP) scenario

SSP5-8.5, representing continued fossil fuel development[17,18]. An overview schematic of the workflow and steps in the analyses are in Extended Data Figure 1.

1. Defining climate vulnerability: data, indices, and dimensions

Holistic principles guide the CCVA and CCRA that we developed: climate change impacts on species are complex and synergistic[*e.g.* 19]. Therefore, the climate vulnerability of species can't be adequately defined by a single index or dimension. Building on this idea, our framework defines vulnerability hierarchically: vulnerability is calculated from its three accepted dimensions (sensitivity, exposure, adaptivity)[7], each of which is derived from four climate indices (12 indices total), which in turn are calculated using data and ecological theory (Table S1). Indices related to species climate sensitivity included species' thermal safety margins[9,20–22], vertical habitat variability and use[23–26], conservation status[27], and cumulative impacts[28–35]. Indices of species climate exposure were calculated from ensemble climate projections and included the species' time of climate emergence from their thermal niche[36–39], suitable thermal habitat loss[40–42], climate-related ecosystem disruption[43–46], and the projected climate velocity[7,47–49]. Indices related to species adaptivity to climate change included the species' geographic range extent[23,47,49,50,52–54], geographic habitat fragmentation[10,55–59], maximum body length[4,10,57,60–64], and historical thermal habitat variability and use[10,65–68]. These climate indices were selected based on pre-defined criteria, as follows: We prioritized indices that are grounded in ecological theory, widely accepted, and validated, preferably through peer-review and publication. Indices were restricted to those where the mechanism of climate change effects was widely accepted and well documented in existing climate change vulnerability studies[20,33,36,38,*e.g.* 47,49,69,70]. Indices were also chosen to maximize their unique information content and minimize redundancies; their uniqueness was evaluated by testing their collinearity and through sensitivity analyses (see Quality control and sensitivity analyses section). Parsimony was also critical: indices that were easy to interpret and calculate were given priority. Our framework constitutes a 'combined approach'[4–6]; it integrates trait-based, correlative, and mechanistic information and incorporates abiotic, biotic, and human pressures acting across multiple biological organization levels (species to ecosystems). The selected indices (Table S1) are described in the Calculation of the indices section.

Table S1 | Indices used in this study.

Index	Description	Data sources	Rationale	References
Sensitivity (S)				
Thermal safety margin	Difference between maximum environmental temperature and species upper temperature tolerance.	AquaMaps Reynolds daily SST	Species inhabiting waters at their upper thermal limits are more vulnerable to further warming. The thermal safety margin has been extensively used in climate vulnerability assessments to measure species sensitivity and tolerance to further warming.	[9,20–22,71,72]
Conservation status	Assessed species extinction risk (categorical).	IUCN red list status	Climate effects on and species can be more severe when species are or have been impacted by additional stressors (*e.g.* fishing, pollution, and nutrient loading) and are at low conservation status.	[27,71]
Cumulative impacts	Multivariate index of human impacts.	Human impact index	Species exposed to multiple impacts are more sensitive to additional stressors, tipping points, synergistic impacts.	[28–35,73]
Vertical habitat variability and use	A bivariate function of maximum depth of occupancy and vertical range of species.	AquaMaps FishBase SeaLifeBase	Habitat generalist species are more adapted to climate variability and change than are specialist species due to their ability to occupy a greater variety of habitats. Species inhabiting the upper ocean and with narrow vertical habitat, ranges are more sensitive to upper ocean warming.	[23–26,66]
Adaptivity (AC)				
Geographic range extent	A bivariate function of the global present-day geographic habitat area and latitude span occupied by the species.	AquaMaps	Broadly distributed species are less susceptible to adverse climate change events over parts of their geographic distributions. Greater opportunity for favourable habitat (*e.g.* climate refugia) within larger distributions.	[10,23,76,26,53,54,57,61,71,74,75]
Geographic habitat fragmentation	The proportion of species native geographic distribution that is fragmented.	AquaMaps	Species with less fragmented habitat ranges have greater access to potentially favourable habitats (*e.g.* climate refugia), migration corridors, and larval dispersal. Consequently, studies in terrestrial and marine systems have reported that species with fragmented geographic ranges are more sensitive to and less resilient to climate change impacts	[10,55,79–82,56–59,71,76–78]
Maximum body length	The maximum body length reached globally.	FishBase SeaLifeBase	The maximum size is a predictor of several life-history traits (*e.g.* generation length, time to maturity, intrinsic rate of population increase) that cumulatively define species potential reproductive capacity and population growth rate. The maximum size (length or mass) reached by species has been commonly used as a proxy of extinction risks and vulnerability of species to climate change. Smaller species that tend to be r-selected are viewed as more resilient than larger, k-selected ones.	[4,10,75,83–85,57,60–64,67,71]
Thermal habitat variability and use	A bivariate function of the fraction of total historical temperature habitat within the species recorded thermal preference and the total temperature range experienced by the species across its global present-day geographic range.	Reynolds daily OISST	Species inhabiting more variable thermal environments such as at the range-edges of their geographic distributions are thought to have a greater capacity to adapt to climate change and are believed to be less sensitive to it	[10,65–68,86–89]
Exposure (E)				
Projected climate velocity	The ratio of projected temporal and spatial change in thermal isotherms within the species geographic distribution.	CMIP6 monthly SST	The velocity of climate change (VoCC) represents climatic isotherms' geographic movement over time and is a widely used measure of climate exposure	[7,47,48,90]
Projected ecosystem disruption	For each grid cell across the focal species native geographic distribution, the proportion of all species projected to exceed their thermal tolerances.	CMIP6 monthly SST	Individual species will be impacted by climate-driven ecosystem restructuring via altered predation, prey availability, competition.	[38,43–46,91]
Projected time of climate emergence from species' thermal niche	The year when the projected temperature first exceeds the thermal tolerance of focal species for at least three years in a row.	AquaMaps CMIP6 monthly SST	The time of climate emergence from pre-industrial temperature variability has been widely used as a proxy for climate change timing. The time of climate emergence from a species thermal tolerance range has recently been developed as an index of the timing of species exposure to dangerous climate conditions.	[36,38,39,49,92]
Projected loss of suitable thermal habitat	For each focal species, the proportion of native geographic distribution lost due to projected climate change.	AquaMaps CMIP6 monthly SST	Species that are projected to lose more of their thermal habitat are more vulnerable.	[40–42,93,94]

2. Data compilation

Overview

The data layers required to calculate the indices in Table S1 were obtained from publicly available and validated sources (Table S2) and were used to calculate the 12 indices of the sensitivity, adaptivity, and species' exposure to climate change. These data sources and indices combined information at the individual species level (*e.g.*, thermal preferences and tolerances, geographic distribution characteristics, trait information, and conservation status) with information about their environment (historical, present and projected thermal habitat, exposure to anthropogenic exposure stressors). Following most previous CCVAs, sea surface temperature (SST) was the primary indicator of climate change[4–6,*e.g.* 8–10,95,96], even though it may not capture every aspect of climate vulnerability[97]. SST is widely available over historical and future projections at high spatial and temporal resolutions. There is a greater understanding of SST's effects on species relative to other climate change variables (*e.g.* net primary production, oxygen concentration, acidification)[19,98]. For these reasons, most CCVAs have used temperature as the primary index of climate change[4–6,*e.g.* 8–10,95,96]. Following this, species that did not inhabit the upper 100m of the ocean were excluded from the analyses, as were those whose maximum depth of occurrence exceeded 1000m, as surface temperatures could weakly define the vulnerability of these species. See Criteria for species inclusion section for a validation of this threshold.

Table S2 | Data sources used in this study.

Type	Variable	Source	Temporal	Spatial	References
Taxonomic, spatial	Species native geographic distribution	AquaMaps	2000-2014	0.5°	[99]
Taxonomic	Conservation status	IUCN Red List	-	-	[69]
Taxonomic	Vertical habitat variability and use	FishBase, SeaLifeBase, AquaMaps	-	-	[99–101]
Taxonomic	Maximum body length	FishBase, SeaLifeBase	-	-	[100,101]
Taxonomic	Thermal niche	AquaMaps	2000-2014	-	[99]
Taxonomic	Species taxonomy	World Register of Marine Species	-	-	[102]
Spatial	Cumulative impacts	Cumulative human impact index	-	$1km^2$	[31–33]
Spatial	Bathymetry	General Bathymetric Chart of the Oceans (GEBCO)	-	$4km^2$	[103]
Spatiotemporal	Sea surface temperature	NOAA daily Optimum Interpolation Sea Surface Temperature dataset	1981-2020	0.25°	[104]
Spatiotemporal	Projected sea surface temperature	Coupled model intercomparison project phase 6 (CMIP6)	1850-2100	1°	[105]

Species native geographic distribution

This CCRA framework required the native geographic distributions of each marine species; these were obtained from the AquaMaps website[99]. AquaMaps predicts marine species' spatial distribution on a 0.5° global grid using environmental niche models experts can validate as a quality control measure (Figure S1). The approach matches observed species occurrence records with local environmental conditions to estimate suitable habitat conditions (environmental envelopes). The niche models predict the relative probability of occurrence and habitat suitability for each species as functions of bathymetry, water temperature, salinity, primary production, and the presence of and for some species, the proximity to sea ice and coasts, and

dissolved oxygen levels. Species occurrence records are obtained through online species databases such as the Ocean Biodiversity Information System (OBIS) or the Global Biodiversity Information Facility (GBIF), while information on the maximum distribution extents and habitat use of species come from FishBase[100], SeaLifeBase[101], and AlgaeBase[106]. Modelled species distributions are harmonized with the currently known species distributions in geographic space, while experts can also review and verify predicted environmental envelopes in environmental space. The predicted distributions for each species are updated every 1-2 years as new data become available. AquaMaps native geographic distribution estimates have been validated using independent survey observations[107] and evaluated against alternative methodologies and independent species distribution datasets[108].

Climate vulnerability and risk were evaluated at 1° resolution to increase the global analyses' computational efficiency and ensure that they were compatible with the spatial resolution of the input climate projections (Table S2). To achieve this, the geographic distributions for each species were rescaled from the native 0.5° resolution using bilinear interpolation. We verified that the bilinear interpolation was suitable through sensitivity analyses by comparing the interpolated probabilities of occurrence from bilinear, nearest neighbour, and spatially averaged approaches and the native 0.5° resolution data. Values interpolated using bilinear and averaging were almost identical (r=0.98), but those from nearest neighbour yielded slightly less similar values (r=0.93). Comparing the interpolated values to the native 0.5° values (one-to-many merge) indicated that the bilinear and average approaches yielded less bias than the nearest neighbour.

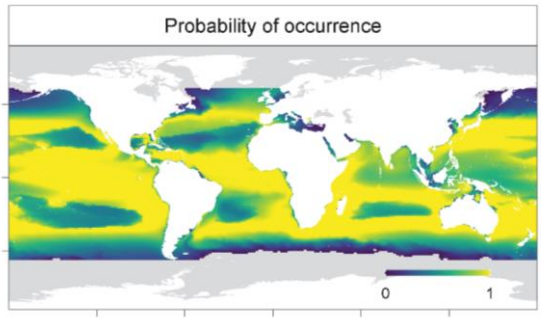

Figure S1 | Example of estimated native geographic distribution for Shortfin mako.
Colours are the probability of occurrence for shortfin mako estimated by AquaMaps[99], where yellow is the highest and blue lowest probability.

Species traits

Thermal niches

The upper and lower thermal preferences and tolerances that define the realized thermal niche of marine species were obtained from AquaMaps[99]. The minimum and maximum temperature preferences for species were defined by the 10th and 90th percentiles of the observed temperature variation from available species occurrence records located within a species' maximum distribution extent, respectively. The minimum and maximum temperature tolerances for species were determined by the 25th and 75th percentiles of the temperature variation, respectively, + 1.5 × interquartile or absolute maximum in extracted data (whichever

is greater). The upper-temperature tolerance values are relevant to this study as they are used to calculate several of the climate indices; these values represent the species realized, rather than fundamental, upper thermal tolerances. To evaluate the veracity of the species' upper thermal tolerances in AquaMaps, we compared them against the fundamental critical thermal maximum for those species that have been determined through experimentation, compiled, and published[9,20,109]. Specifically, we compared the upper realized thermal tolerances reported in AquaMaps against the fundamental thermal tolerances for 60 matching species in the GlobTherm database[109], 76 species reported in Pinsky *et al.* [20], 58 species reported in Comte *et al.* [9], and 767 species that were imputed in Comte *et al.* [9]. The AquaMaps realized upper thermal tolerances were positively correlated to the fundamental upper thermal tolerances in the published databases (r=0.8-0.88; Figure S2). However, as expected, the fundamental tolerances were generally higher than the AquaMaps realized tolerances. This discrepancy may be driven by the difference in the duration of thermal exposure. Whereas realized tolerances were evaluated using time-averaged SST, fundamental tolerances are derived from experiments that capture more acute heat exposure (*e.g.* responses over minutes, hours, days). Were we to use the hottest hourly or daily temperature in a year, we expect the realized and fundamental tolerances would be equivalent.

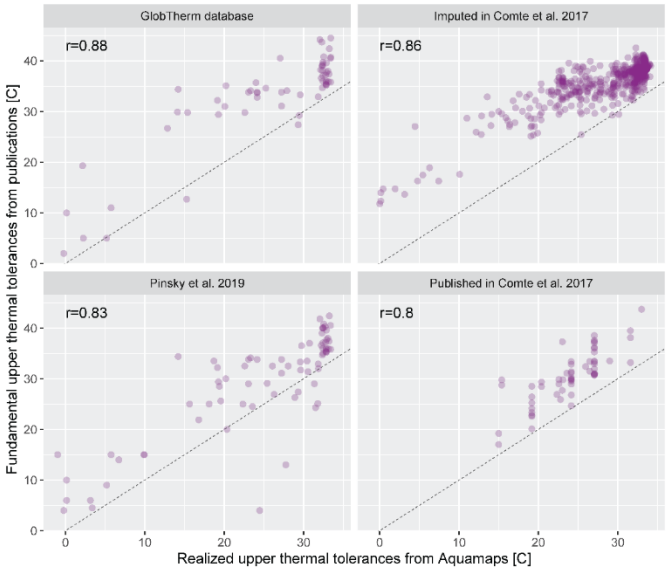

Figure S2 | Relationships between realized upper thermal limits of species in AquaMaps and in the scientific literature. Points show the upper thermal tolerances of species reported in AquaMaps against matching species from the GlobTherm database [109], Pinsky *et al.* [20], Comte *et al.* [9], and imputed in Comte *et al.* [9]. Dashed lines represent a 1:1 relationship.

Maximum body lengths

The maximum body size of species was estimated from the FishBase[1] and SeaLifeBase[2] databases. From FishBase, length-length relationships were used to calculate maximum lengths in standard units of total length (TLen). For species with no length-length relationship yet in FishBase, relationships were established

[1] http://www.fishbase.org
[2] https://www.sealifebase.ca/

using measurements in the MORPHOMETRICS table or the PicturesMain tables. Where needed, lengths from the DIET, FECUNDITY, MATURITY, OTOLITH, POPCHAR, POPLL, POPLW, and SPAWNING tables were compiled and converted to TLens. To validate the length records, the largest maximum lengths were examined to find and exclude those which are not plausible for each genus. Maximum lengths from FishBase were obtained from R. Reyes Jr at Quantitative Aquatics, Inc. From SeaLifeBase, the type of measurement used to assess maximum total lengths (TLens) for invertebrates depended on their taxonomy. TLen was defined by the shell length and body length for gastropods, bivalves, and some decapods. TLen was determined by mantle length (ML) for cephalopods, carapace length (CL) for decapods, and shell height (SHH) for some gastropods. The lengths (TLen, ML, CL, SHL) across tables were then compared, and the larger lengths were used to update the maximum lengths in the SPECIES table. P.M. Sorongon-Yap compiled maximum lengths from SeaLifeBase at Quantitative Aquatics, Inc.

Fuzzy matching species traits

Species-level information (*e.g.* traits) were combined within the database according to their Latin species names. However, in some instances, the same species were entered differently between the different data sources; they were synonyms to their accepted taxonomies or were entered incorrectly due to human error. The World Register of Marine Species (WoRMS)[102] was used as a taxonomic template to validate all species' identities and ensure that the taxonomies were correct and standardized across the different data sources. WoRMS contains both the accepted Latin and common names of all available species and their known synonyms. Using fuzzy string matching, species-level climate indices were joined according to species identity. Using the IUCN Red List conservation status as an example, the fuzzy string distance between each Red List species and each WoRMS synonym was calculated; this value is 0 when the WoRMs and Red List Latin names are identical, 1 when there is a one-character difference, and so on. We then selected the most likely match between WoRMS and the Red List Latin names according to the minimum string distance, provided that the distance was <=1. The distance of 1 was selected with the understanding that human error (*e.g.* data entry typos) would most likely result in single character omissions, insertions, and substitutions.

Environmental conditions

Temperature conditions were evaluated using daily SST estimates from the NOAA 0.25° daily Optimum Interpolation Sea Surface Temperature dataset (OISST)[104]. The temperature dataset is a combination of observations from different observation platforms (satellites, ships, buoys, and Argo floats) and is available globally since 1981 at a spatial resolution of 0.25°. SST values were rescaled to a global 1° grid using bilinear interpolation.

A multivariate index of cumulative human impacts (HI) on ocean ecosystems was developed in Halpern *et al.* [31,33]. The HI index integrates 17 global anthropogenic drivers of ecological change, including fishing pressure, pollution, invasive species, eutrophication, climate change, and others. The HI estimates

were available at a global 1km^2 native resolution. These values were rescaled to a global 1° grid using bilinear interpolation.

Climate projections

We obtained monthly time-series of projected monthly SST from the coupled model intercomparison project phase 6 (CMIP6) between 1850 and 2100. All SST projections were interpolated to a regular global 1x1° grid. An ensemble of SST projections was obtained from 15 published Global Climate (GCM) or Earth System Models (ESMs) within the CMIP6 archive (Table S3). These models span a broad range of the projections of SST within the CMIP6 model set. SST projections (°C) were made under the IPCC's shared socioeconomic pathway (SSP) scenarios SSP5-8.5, representing continued fossil fuel development, and SSP1-2.6, representing an increase in sustainable development[17,18].

Table S3 | List of models from the CMIP6 multi-model ensemble archive used in this study.

N	Model	Modeling Center (or Group)	Reference
1	BCC-CSM	Beijing Climate Center	110
2	INM-CM4-8	Institute for Numerical Mathematics	111
3	MIROC6	Japan Agency for Marine-Earth Science and Technology	112
4	MRI-ESM2-0	Meteorological Research Institute	113
5	ACCESS-CM2	Commonwealth Scientific and Industrial Research Organisation	114
6	CAMS-CSM1-0	Chinese Academy of Meteorological Sciences	115
7	CMCC-CM2-SR5	Centro Euro-Mediterraneo sui Cambiamenti Climatici	116
8	FGOALS-f3-L	Chinese Academy of Sciences	117
9	FIO-ESM-2-0	First Institute of Oceanography	118
10	KACE-1-0-G	National Institute of Meteorological Research & Korean Meteorological Agency	119
11	KIOST-ESM	Korea Institute of Ocean Science and Technology	120
12	NESM3	Nanjing University of Information Science and Technology	121

3. Calculation of the indices

Overview

Climate indices were calculated or obtained in their native units. Each vulnerability index was defined by the focal species' traits, calculated from environmental or ecological data on a geographic grid across the geographic distribution of the focal species and/or a combination of the two. This resulted in indices that were both taxonomically (*e.g.* each species) and geographically (*e.g.* each grid cell and species) explicit. The indices were then transformed to ensure they mapped onto a standardized scale (range: 0-1), using hyperbolic functions (see section Notes on standardization, below). This critical step ensured that indices with different units could be compared, normalized, and combined. It also ensured that vulnerability could be re-estimated at different spatial resolutions or at different points in time without a loss of information. The following section describes the interpretation, calculation, and standardization for each index.

Notes on standardization: reference values and scaling

The indices of climate sensitivity, exposure, and adaptivity described below were in different units, and standardizations were necessary to ensure that all indices were directly comparable on a standardized scale

and their interpretations were ecologically grounded. Furthermore, the indices needed to be calculated in this manner to ensure that the CCRA could be reproduced in future studies, potentially over different geographic domains (*e.g.* regional), at higher spatial resolutions, and at different future exposure horizons without any loss of information. The indices also needed to be calculated so that vulnerability could be monitored over time. *Reference values* and *scaling functions* were used to meet these criteria.

Reference values were used to ensure that the indices varied on standard interpretable scales (0-1). They were selected using established guidelines such as spatial or taxonomic comparison against global maximum[32,122]. Alternatively, scaling functions described how the scaled indices varied as their unscaled analogues increased. It was possible to scale some indices using standard approaches (*e.g.* $\log_{10}$) and/or by expression as a proportion of a global or theoretical maximum (*e.g.* %). Other indices were scaled using rectangular hyperbolic functions that characterize the change in the indices from the height of an asymptote and the rate at which it is reached. Rectangular hyperbola is also known as saturating hyperbola, decelerating curve, and asymptotic regression, representing one of the most ubiquitous curves in biology[123]. They have been used to describe a variety of biological phenomena, including, for instance, the reaction speed of enzymes, the nature of predator-prey interactions, and ecosystem stability. Here we use hyperbolic functions described by the exponential equation due to their wide use and ease of interpretation to standardize and normalize some climate indices. The exponential growth function is described as

$$Y = \alpha e^{\lambda X}, \qquad \text{Equation 1}$$

where α is the y-intercept and λ is the rate parameter. The equation ensures that Y ranges between 0 and ∞ and increases for λ>1 and declines for λ<0. Changing these two parameters can yield widely varying response functions. For example, an asymptotic increase in Y can be described by,

$$Y = 1 - e^{-\lambda X} \qquad \text{Equation 2}$$

where higher values of λ yield sharper increases, and earlier asymptotes in Y with lower values yielding slower increases that do not reach an asymptote **(**Figure S3**).**

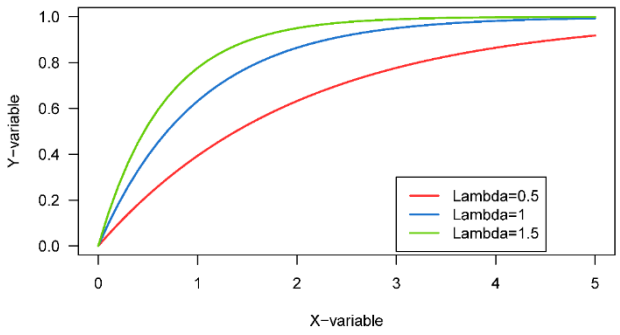

Figure S3 The exponential curves described by Equation 1 under different levels of λ.

This generalized exponential function was used to define the scaling of the indices and ensure they were standardized between 0 and 1. These standardizations are defined in the descriptions of the individual indices; sensitivity analyses evaluating the validity of their use are described in the Quality control and sensitivity analyses section below.

Climate sensitivity indices

Overview

The species' sensitivity quantifies their responsiveness to climate change and is comparable to the concept of reactivity in community ecology[14,124]. The species' sensitivity is primarily a function of the present environmental conditions and status of the species. For instance, these include their environment's status, the stressors they are presently exposed to, their current conservation status, and their physiological condition.

Thermal safety margins

Rationale

The thermal safety margin (TSM) has been extensively used in climate vulnerability assessments to measure species sensitivity and tolerance to further warming[9,20,21]. Species inhabiting thermal environments close to their upper temperature limit (narrow thermal safety margin) are more vulnerable to climate warming than those further away (Figure S4).

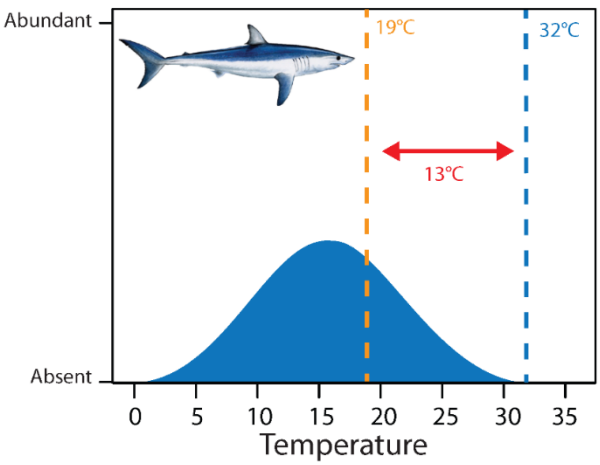

Figure S4 | Thermal safety margin.
The thermal safety margin for shortfin mako in grid cell *c* (red arrow) is calculated as the distance between the current warmest temperatures experienced in grid cell *c* (orange vertical line) and the maximum temperature tolerance of shortfin mako (blue shaded density and vertical line).

Calculation

For each species within each 1° grid cell across its estimated geographic distribution, a thermal safety margin was calculated as the difference between the estimated upper thermal tolerance of the species and the maximum daily SST observed over the previous decade (*e.g.* here, between 2010 and 2020). AquaMaps provided the estimated thermal tolerances and native geographic distribution for each species. NOAA daily Optimum Interpolation Sea Surface Temperature (OISST) estimates were used to evaluate the maximum temperatures reached across each species' geographic distribution between 2010 and 2020[104](Table S2). The standardization function allowed climate sensitivity to increase exponentially as the TSM declined as

$$S\,TSM_{s,c} = e^{-\lambda TSM_{s,c}}, \qquad \text{Equation 3}$$

where $TSM_{s,c}$ is the thermal safety margin (°C) for species s in grid cell c, and λ is the rate parameter (0.33). The rate parameter (λ) and resulting equation were chosen to standardize the index (0-1), normalize it's distribution and allow most of the change in sensitivity to occur for TSMs below 10°C, with sensitivity being increasingly uniform when the TSM exceeds 10°C. There should be little difference in the sensitivity of species inhabiting ocean temperatures that are >10°C from their upper thermal maximum (Figure S5). Our definition of sensitivity (Equation 3) assumes that risk declines with thermal distance from the species' upper thermal tolerance. In general, thermal performance is strongly warm skewed, with fitness expected to increase gradually until the thermal optima before rapidly declining to zero as the species' upper thermal tolerance limit approaches. Our assumption that risk increases continuously with temperature thus captures the risk of the species' upper thermal tolerance being exceeded rather than representing variation fitness within the thermal niche. Refer to the Quality control and sensitivity analyses section for an evaluation of how the vulnerability calculations are affected by the specification of λ.

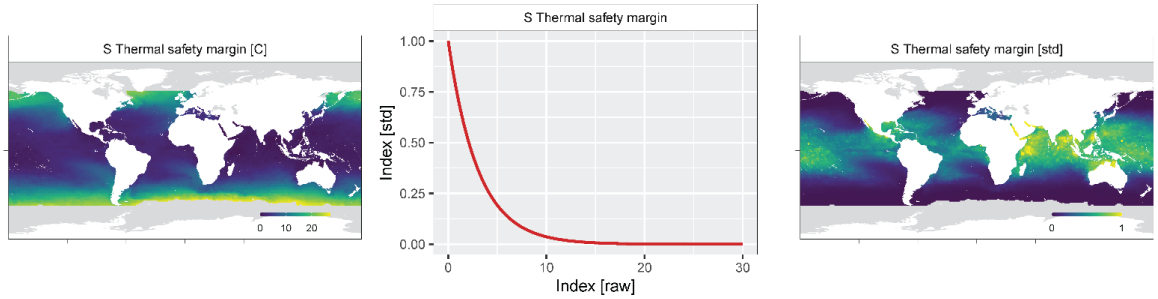

Figure S5 | Thermal safety margins for Shortfin mako.
The thermal safety margins (left) were calculated across the native geographic distribution and transformed using the function described by Equation 3 (middle) to standardize them (right).

The transformation altered the distribution of the TSMs such that they were less skewed (Figure S6)

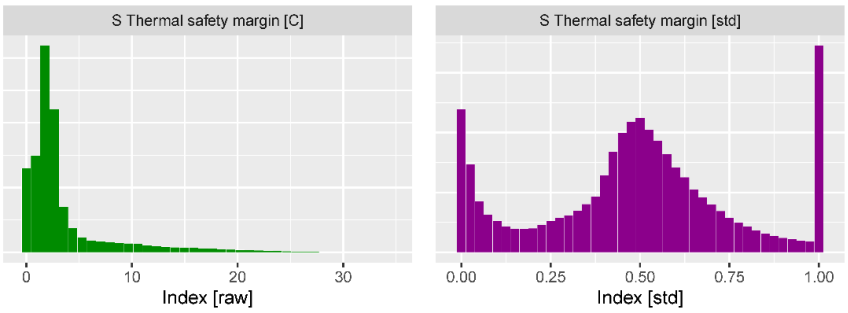

Figure S6 | Distribution of thermal safety margins.
Histograms depict the distribution of thermal safety margins for species and locations randomly sampled before (green; left) and following (purple; right) standardization. The distributions were derived from random samples of 10 M observations.

Conservation status of species

Rationale

The estimated conservation status of individual species was obtained from the IUCN Red List Index of species (RLI)[69], the world's most comprehensive inventory of biological species' global conservation status. The Red List classifies species into extinction risk categories based on population trends, population size and structure, and geographic distribution, and the process is quality controlled through a peer-review

process. Red List assessment contributors include BirdLife International, the Institute of Zoology, the UNEP World Conservation Monitoring Centre, and the IUCN Species Survival Commission. The IUCN strives to update each species assessment every five or ten years. Excluding species that have not been evaluated or that are data deficient, species are categorized as extinct, extinct in the wild, critically endangered, endangered, vulnerable, near threatened, or of least concern (Figure S7).

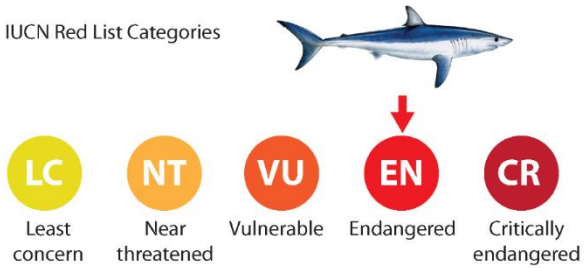

Figure S7 | IUCN conservation status.
The spectrum of IUCN conservation status categories is depicted with shortfin mako classified as 'endangered.'

Calculation

The Red List categories were transformed to numeric values as follows: Critically endangered=0.5, endangered=0.05, vulnerable=0.005, near threatened/lower risk/near threatened=0.0005, least concern/lower risk/least concern=0; they were then standardized between 0-1 (Figure S8).

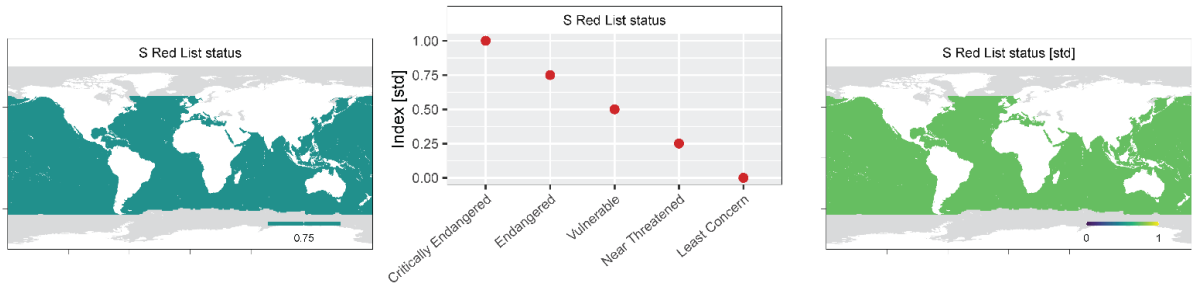

Figure S8 | IUCN Red List categorization for Shortfin mako.
The Red List classification for shortfin mako was converted from discrete categorical responses (left panel) to standardized numeric values (middle and right).

The Red List values were skewed such that most species had a low sensitivity ('least concern'); (Figure S9)

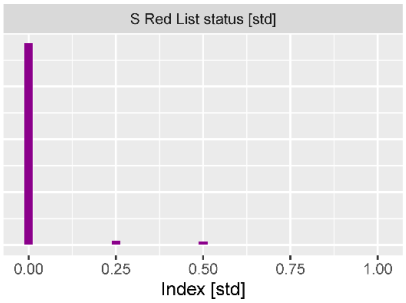

Figure S9 | Distribution of IUCN Red List status values. Histograms depict the distribution of Red List status for species after standardization.

Cumulative impacts

Rationale

Climate effects on ecosystems and species can be more severe when overlaid by additional stressors, such as fishing, pollution, and nutrient loading. For example, Ottersen *et al.* [34] reported that extensive fishing could render fish populations less resistant to the harmful effects of short-term climate variability on occasional low year classes. Alternatively, studies have reported that species and ecosystems protected from such stressors may be more resistant and resilient to stressors such as climate change and fishing[28–30]. For example, Le Bris *et al.* [35] found that management initiatives to protect large female lobsters in the Gulf of Maine (GoM) have led to higher resilience to ocean warming and productivity of the lobster population there when compared to populations in adjacent Southern New England, where large individuals were less strictly conserved[35]. Without conservation measures to protect large lobsters and female reproductive lobsters, lobster abundance in the GoM would have increased by 242% rather than 515%, as oceans warmed between 1985 and 2014[35]. These results contribute to a growing body of research suggesting that protecting species, and predators, in particular, can enhance the resilience of populations to stressors, such as climate change[14,35,125].

Calculation

The multivariate index of cumulative human impacts (HI) on ocean ecosystems developed in Halpern *et al.* [31,33] was used as an index of cumulative impacts on marine ecosystems. The HI index (HII) integrates 17 global anthropogenic drivers of ecological change, including fishing pressure, pollution, invasive species, eutrophication, climate change, and others. The 1km^2 HI values were re-interpolated using nearest neighbour methods to a worldwide 1° grid. This interpolation changed the HII scale: whereas the native 1km^2 HII ranged between 0-12, the interpolated HII ranged from 0-8. The range of the HII may likely change as it is updated. HII was transformed to ensure that it would be insensitive to the native scale, as

$$S\,HII_c = 1 - e^{-\lambda HII_c}, \qquad \text{Equation 4}$$

where HII_c is the HII in cell c, and λ is the rate parameter, set to 0.6. The rate parameter (λ) and resulting equation were chosen to standardize the index (0-1), normalize it's distribution and ensure that $S\,HII_c$ ranges between 0 and 1 and is nearly uniform for values above 5 (Figure S10). Refer to the Quality control and

sensitivity analyses section for an evaluation of how the vulnerability calculations are affected by the specification of λ.

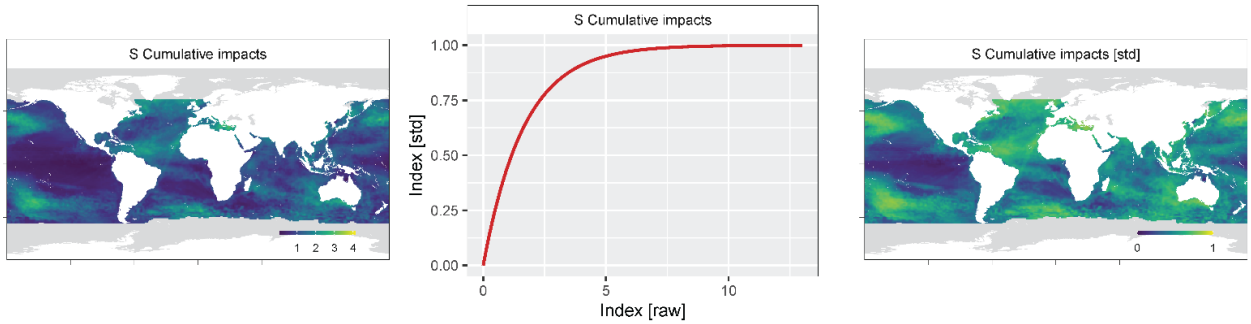

Figure S10 | Cumulative human impacts across the native geographic distribution of Shortfin mako. The HII across the native geographic distribution of shortfin mako (left) were transformed using Equation 4 (middle) into standardized values (right).

The distribution of the cumulative impacts is shown before and after transformation (Figure S11).

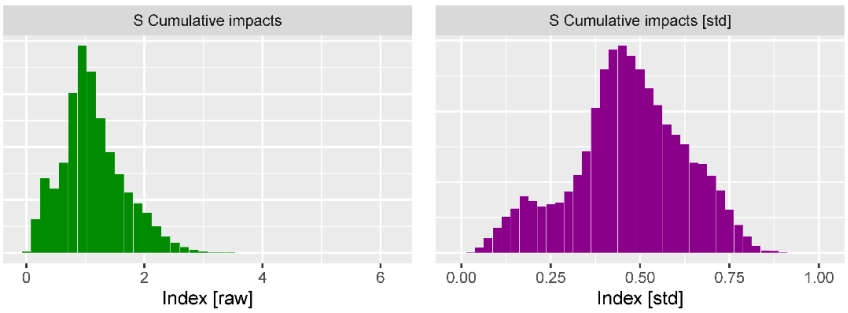

Figure S11 | Distribution of cumulative human impacts. Histograms depict the distribution of cumulative human impacts before (green; left) and following (purple; right) standardization.

Vertical habitat variability and use

Rationale

Habitat generalist species are more adapted to climate variability and change than are specialist species due to their ability to occupy a greater variety of habitats[23–26]. Vertical habitat specialization, the depth of species occupancy, and the ability to occupy different vertical habitats play a significant role in determining the adaptivity of species to climate change. Species restricted to the uppermost epipelagic layers of the ocean are expected to have a lower capacity to adapt to climate change, as the upper oceans are more exposed to warming [e.g. 10]. Similarly, species that occupy a narrow range of vertical habitats are also less adaptable. As such, a vertical habitat index was calculated for each species according to its maximum occupancy and range depth.

Calculation

Our analysis included species that inhabited the upper 100m of the ocean and excluded those whose maximum depth of occurrence exceeded 1000m (excepting mammals and deep-diving pelagics such as tunas and billfishes); surface temperatures could weakly define the climate risk of these species. . For these species, climate sensitivity to upper ocean warming declined exponentially with both the maximum depth of occupancy and vertical range of each species as

$$SVR_s = e^{-\lambda VR_s} \qquad \text{Equation 5}$$

$$S\,Mdep_s = e^{-\lambda Mdep_s}$$ Equation 6

where VR_s and $Mdep_s$ are the vertical range and maximum depth of occupancy for species s in meters, and λ is the rate parameter (0.003). The rate parameter, λ, corresponds to the rate of decline in climate sensitivity over depth and depth range and was empirically derived as the exponential rate of change in the difference between surface and subsurface temperatures across depths between 0 and 1000m globally. These equations allow sensitivity to scale between 0 and 1, with most of the change in sensitivity occurring between the surface and 500 m depth or range, with sensitivity being very similar below 500 m (Figure S12). Maximum sensitivity occurred for surface-dwelling species with narrow vertical ranges, while the lowest sensitivity occurred for species below 500 m with wider vertical ranges. Estimates of maximum depth of occupancy and vertical habitat range were retrieved from AquaMaps[99] and FishBase[126]. The maximum depth of occupancy and vertical habitat range was truncated by the maximum bathymetry present in each grid cell across its native geographic distribution for each species. Bathymetry values were extracted from the General Bathymetric Chart of the Oceans (GEBCO; Table S2). Cumulative climate sensitivity was then calculated as the mean of the species' standardized vertical range (Equation 5) and the maximum depth of occupancy (Equation 6) indices. Refer to the Quality control and sensitivity analyses section for an evaluation of how the vulnerability calculations are affected by the specification of λ.

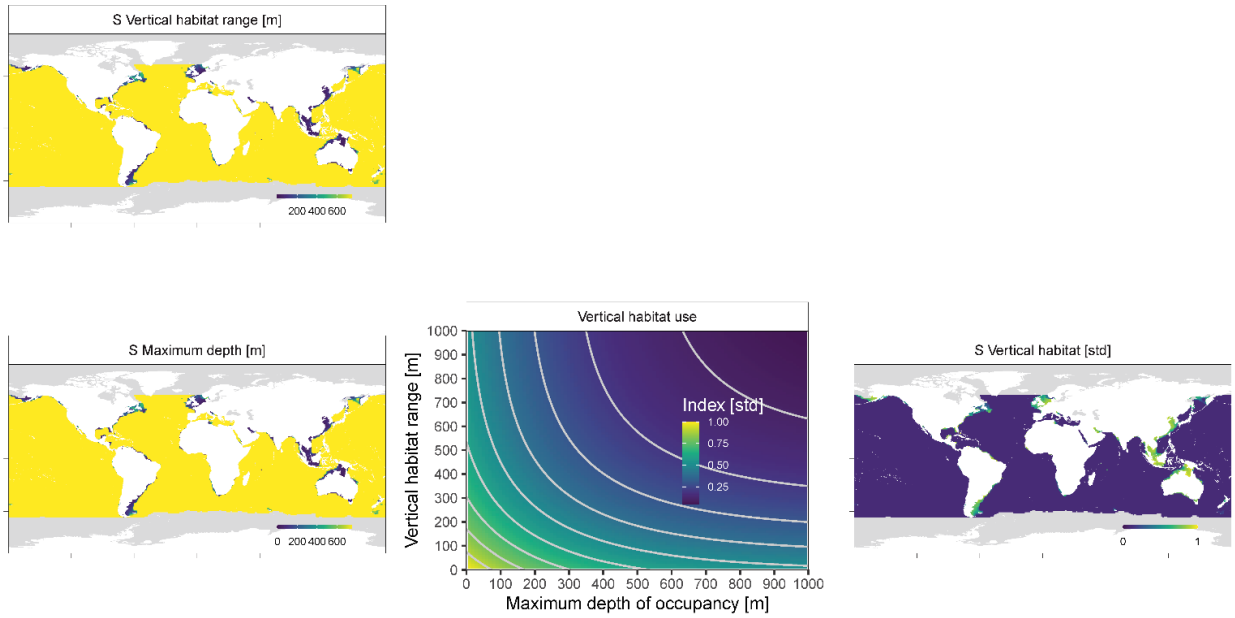

Figure S12 | Vertical habitat use of Shortfin mako.
The maximum depth of occupancy and vertical habitat range (left) were transformed using the function described by Equation 6 (middle) to develop a standardized index of vertical habitat use (right panel). The transformation function (Equation 6; middle) specifies that species restricted to the oceans' uppermost layer are most sensitive to upper-ocean warming (middle). The sensitivity declines rapidly below 500 m and is virtually nonexistent below 1000 m depth.

The distribution of the vertical habitat range and the maximum depth of species are shown before and after transformation (Figure S13).

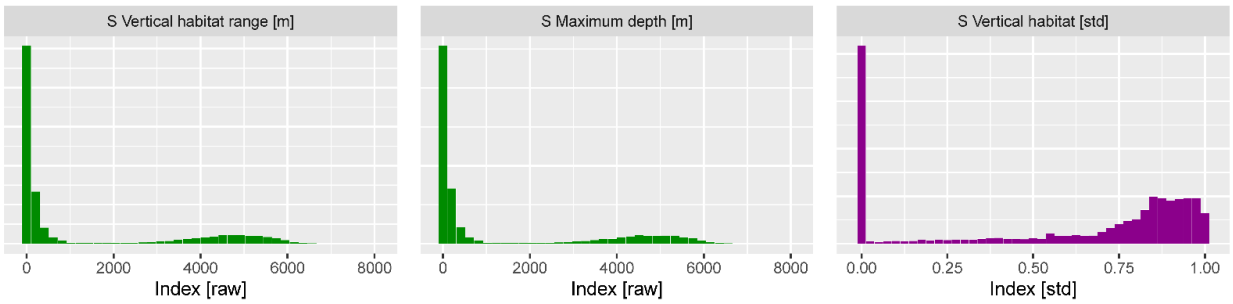

Figure S13 | Distribution of vertical habitat uses.
Histograms depict the probability distribution of vertical habitat range (green; left), maximum depth of occupancy (green; middle), and the standardized vertical habitat index (purple; right).

Climate exposure indices

Overview

The exposure of species to climate change is primarily a function of the future conditions of their environment. Accordingly, the exposure of species to future climate changes was evaluated using monthly projections of sea surface temperature (SST) between 1850-2100 from Global Earth System Models (ESMs) in the coupled model intercomparison project phase 6 (CMIP6). All SST projections were regridded onto a regular global 1x1° grid. Each exposure index (see below) was first calculated separately for each ESM projection on a global grid. Following this, the multi-model ensemble average for each separate exposure index was calculated. Each exposure index was standardized by a normalization constant to facilitate comparability when using alternative data sources or spatial resolutions. The cumulative climate exposure was then estimated as the average across all standardized exposure indices. Lastly, the climate exposure for each species within each 1° grid cell was obtained by calculating the probability of species occurrence by the standardized climate exposure in that grid cell.

Projected time of climate emergence

Rationale

The time of climate emergence from pre-industrial temperature variability has been widely used as a proxy for climate change timing[36,49,92]. In the same vein, the time of climate emergence from a species' thermal tolerance range has recently been developed as an index of the timing of species exposure to dangerous climate conditions[38,39]. This index provides a means of assessing whether exposure to hazardous climate change is an imminent or distant threat (Figure S14).

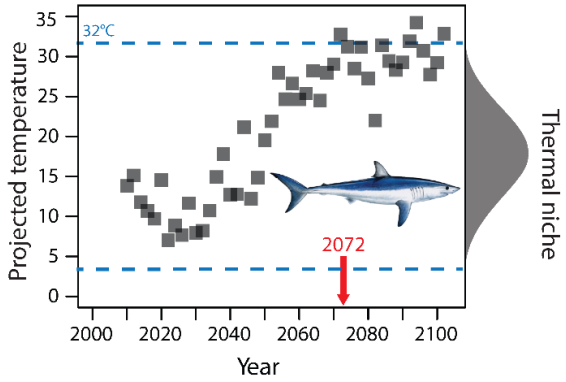

Figure S14 | The timing of climate emergence from the thermal niche. The time of emergence for shortfin mako in grid cell *c* (ToE; red arrow) was calculated as the year in which the projected annual maximum of monthly temperature within grid cell *c* (points) first exceeds the thermal niche of shortfin mako (gray shaded density and blue horizontal line).

Calculation

The time of initial climate emergence (ToE) for each species was estimated as the year in which the projected maximum annual of monthly SST emerges from the species thermal tolerance niche for two consecutive years. ToE calculations were made using the methods described in Trisos *et al.* [38] for each species within each 1° grid cell across its native geographic distribution. Whereas Trisos *et al.* [38] used projections of mean annual temperature and an exceedance run length of 5 years, we used temperature of the hottest month and a run length of two years; in doing so, our ToE index quantifies the onset of thermal stress in species rather than absolute mortality to inform climate risk. We used climate projections between 2015 and 2100. ToEs for species that did not exceed their thermal tolerances within this projection window were set at the maximum year of the projection. The ToE for each species and grid cell was estimated individually for each ESM and then averaged across all ensemble models. The resulting ToEs were standardized according to

$$E\,ToE_{s,c} = e^{-\lambda ToE_{s,c}}, \qquad \text{Equation 7}$$

where $ToE_{s,c}$ is the ensemble projected year of climate emergence from the thermal niche for species *s* in grid cell *c*, and λ is the rate parameter (0.033). The rate parameter (λ) and resulting equation were chosen to ensure that $E\,ToE_{s,c}$ ranges between 0 and 1, and increases more rapidly as it approaches 0 and declines more slowly as it increases (Figure S15). Maximal exposure occurs for species inhabiting waters that are already thermally hazardous (*e.g.* ToE=0). Refer to the Quality control and sensitivity analyses section for an evaluation of how the vulnerability calculations are affected by the specification of λ.

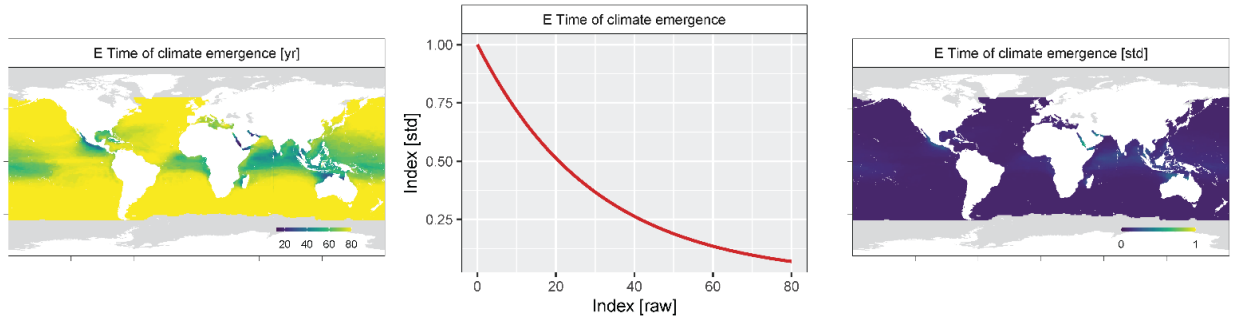

Figure S15 | Projected time of climate exposure for Shortfin mako.
The multi-model projected time of climate exposure (left) was calculated across the native geographic distribution of shortfin mako and transformed using the function described by Equation 7 (middle) to standardize them (right).

The distribution of the projected time of climate emergence of species' thermal niche is shown before and after transformation (Figure S16).

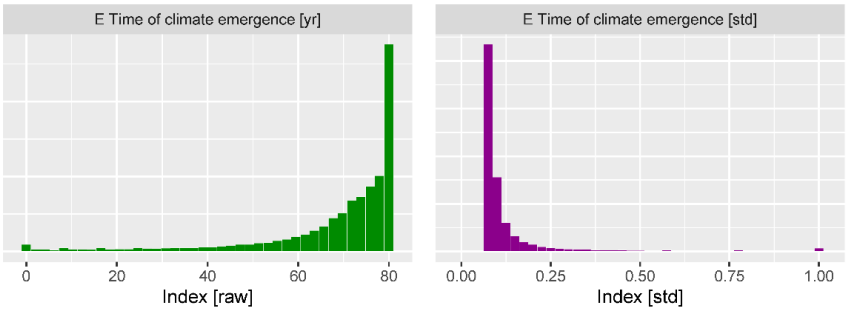

Figure S16 | Distribution of projected time of climate exposure.
Histograms depict the probability distribution of projected time of climate exposure for species and locations randomly sampled before (green; left) and following (purple; right) standardization. The distributions were derived from random samples of 10 M observations.

Projected ecosystem disruption

Rationale

Healthy, intact ecosystems are thought to be more resilient and resistant to stressors, including climate change[91]. Alternatively, stressors such as climate change can erode the structure and function of ecosystem through several pathways. In addition to the direct effects of temperature on species via their physiological tolerances, climate change can also indirectly affect species by altering their predators, prey, and competitors[43–46]. Such ecologically mediated climate change effects on species are notoriously challenging to assess and understand *in situ* due to the presence of lagged effects between predators and prey, the high collinearity between non-interacting species, and the scarcity of requisite data to resolve the effects. Notwithstanding this, studies suggest that changes in abundance or distribution of species can trigger cascading ecosystem effects, ecological regime shifts, and alternative stable states, causing modified ecosystem structure and function[127–129]. Studies also indicate that these ecological effects tend to be more significant when the abundance or distribution of several species changes in concert rather than isolation. Research into biodiversity and ecosystem function also suggests an accelerated risk to ecosystem function as more species are removed from it[28].

Calculation

To quantify the magnitude of ecological disruption resulting from an ecosystem's exposure to climate change, we calculated the fraction of all species in our analysis at each location (grid cell) that are thermally exposed before the maximum year in the projection window (the year 2100). This index quantifies the risk of secondary ecological effects (*e.g.*, changes in predation, prey availability, competition) due to climate change that species may be exposed to; it does not assume all species interact but instead captures the risk that a species will be impacted by the loss of other species in the system, which will increase with the number of species that are exposed

$$E\ ToEE_c = 1 - e^{-\lambda ToEE_c}, \qquad \text{Equation 8}$$

where $ToEE_c$ is the proportion of all species in grid cell c that emerge from their thermal niche by 2100, and λ is the rate parameter, set at 4. The rate parameter (λ) and resulting equation were chosen to standardize the index (0-1), normalize it's distribution and specify that a species' exposure increases asymptotically with the fraction of species lost in its ecosystem, with the most significant exposure occurring for species inhabiting ecosystems with the greatest loss of species. We contend that individual species are likely to be most affected when the ecosystem initially undergoes climate-driven restructuring (species loss); thus, the exposure increases most rapidly for species loss up to ~50%. However, as the climate-driven ecosystem disruption becomes sufficiently large, additional species losses are likely redundant: *e.g.* losing 80% of species is functionally equivalent to losing 90%. Refer to the Quality control and sensitivity analyses section for an evaluation of how the vulnerability calculations are affected by the specification of λ. $ToEE_c$ was estimated individually for each ESM using the approach described in Trisos *et al.* [38] and then averaged across all ensemble models (Figure S17).

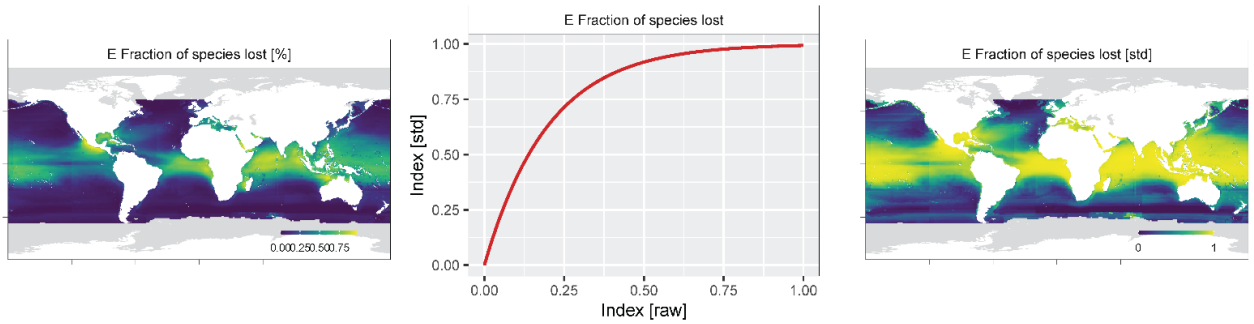

Figure S17 | Magnitude of ecological change across the native geographic distribution of Shortfin mako. The fraction of species projected to be lost in each grid cell were calculated across the geographic distribution of shortfin mako (left) and transformed using the function described by Equation 8 (middle) to standardize them (right).

The distribution of the projected fraction of species lost following transformation is shown in Figure S18.

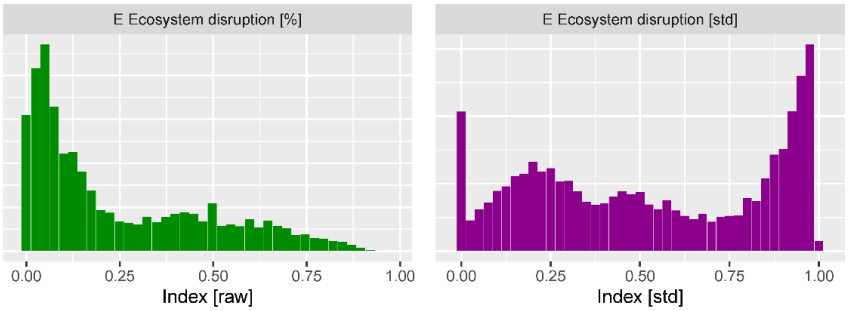

Figure S18 | Distribution of the projected magnitude of ecological changes. Histograms depict the probability distribution of the projected magnitude of species' ecological changes before (green; left) and following (purple; right) standardization.

Projected loss of suitable thermal habitat

Rationale

Temperature changes have, and are expected to continue to cause, geographic range expansions, contractions, and redistributions in marine species[40–42,93]. Accordingly, changes in species' geographic range predicted by temperature changes are frequently used to define their vulnerability to climate change[4,6,42,95]. The nature and magnitude of such geographic range shifts will predominantly depend on the correspondence between local temperature changes and the species' thermal tolerance niche. Accordingly, we evaluated the extent of each species' estimated native geographic distribution that would be lost due to projected ocean warming. We did not assess the net change in the entire geographic distribution of species (*e.g.* the difference between the habitat gained and lost due to climate) for several reasons. While range contractions can be driven by a single variable (*e.g.* temperature), species expansions into new habitats will depend on the favorability of several environmental and biotic factors that we did not evaluate (*e.g.* bathymetry, oxygen, acidity, ocean mixing, predators, prey, competition, dispersal). Evaluating species range expansions would require future projections in many of these environmental and biotic factors, which are, in many cases, unavailable. Even if such projections were available, using them to forecast species range expansions would introduce considerable uncertainty into our analysis. Further, this study aims to assess risk to current marine biodiversity rather than trying to project how biodiversity may shift in the future, which has been the focus of other studies[*e.g.* 130]. Whereas many factors are needed to determine range expansions, the lethality of temperature alone can mediate range contractions. Therefore, our approach is conservative but possibly simplistic for some species, as it predicts that most species will lose habitat but that none will gain. Nonetheless, this index provides a valuable assessment of how the native geographic distribution of species could contract in response to climate change while avoiding the assumptions, complexities, and data requirements required to evaluate the net distributional responses. Finally, given that our framework does not evaluate the potential for geographic range expansions, it is best interpreted as the climate risk to the *in situ* persistence of species.

Calculation

Projected changes in species geographic distributions that are attributable to temperature were estimated from the time of climate emergence from the thermal niche calculations described above. The number of

grid cells in each species native geographic distribution is projected to emerge from their thermal niche prior to the end of the climate projection window (the year 2100) was standardized by the total number of grid cells in their native geographic distribution. This index quantifies the geographic extent of adverse climate change impacts that species may be exposed to.

$$E\,THL_s = 1 - e^{-\lambda THL_s}, \qquad \text{Equation 9}$$

Where THL_s is the proportion of all grid cells across the native geographic distribution of species s that are projected to become thermally hazardous by 2100, and λ is the rate parameter, set at 5. The rate parameter (λ) and resulting equation were chosen to standardize the index (0-1) and specify that a species' exposure increases asymptotically with the fraction of thermal habitat loss, with the most significant exposure occurring for species losing all of their present-day suitable thermal habitats. No transformation was necessary as there was no reason to expect a nonlinear variation in the exposure index as a function of distributional changes (Figure S19). The maximum exposure occurs for species projected to lose all suitable habitats. Refer to the Quality control and sensitivity analyses section for an evaluation of how the vulnerability calculations are affected by the specification of λ. THL_s was estimated individually for each ESM and then averaged across all ensemble models (Figure S19).

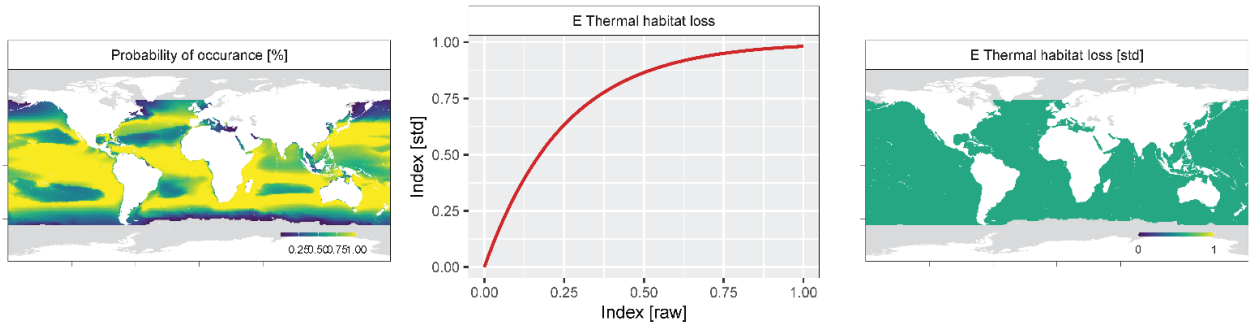

Figure S19 | Thermal habitat loss for Shortfin mako.
The proportion of the entire native geographic distribution of shortfin mako (left) was used to evaluate the projected thermal habitat lost due to climate change (right).

The distribution of the projected thermal habitat loss of all species is shown in Figure S20.

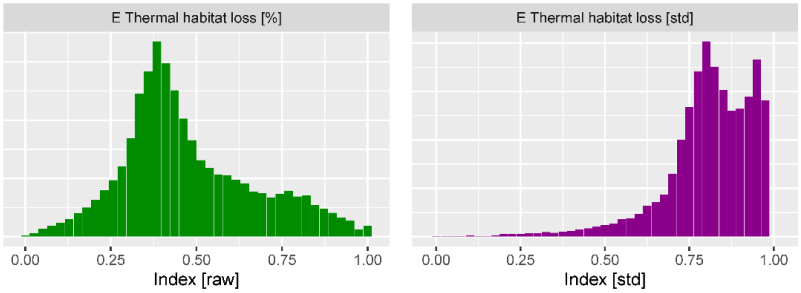

Figure S20 | Distribution of the projected thermal habitat loss. Histograms depict the probability distribution of projected thermal habitat loss following standardization.

Projected climate velocity

Rationale

The velocity of climate change (VoCC) represents climatic isotherms' geographic movement over time and is a widely used measure of climate exposure[7,47,48,90,131]. Species inhabiting waters with greater velocities of climate change are more exposed.

Calculation

For each GCM projection, we calculated climate velocity (km yr^{-1}) over the duration of the climate projection (2015-2100), using a gradient-based approach[48], as

$$VoCC_c = \left|\frac{s_c}{t_c}\right|, \qquad \text{Equation 10}$$

where s_c is the local spatial climatic gradient (°C km) and t_c is the long-term time trend (°C yr-1) in each grid cell, c [47,48]. $VoCC_c$ was calculated on a 3 × 3 cell neighbourhood and averaged across all available GCM models to obtain an ensemble average and its standard error.

$$E\,VoCC_c = 1 - e^{-\lambda VoCC_c}, \qquad \text{Equation 11}$$

where $VoCC_c$ is the VoCC in grid cell c until 2100, and λ is the rate parameter, set at 0.02. The rate parameter (λ) and resulting equation were chosen to standardize the index (0-1), normalize it's distribution and specify that a species' exposure increases asymptotically with the speed at which temperature isotherms are projected to move across the ocean. The most significant exposure occurs in areas with rapid isotherm movement (Figure S21). These calculations were made in the R statistical computing platform using the *VoCC* package[48,132]. Refer to the Quality control and sensitivity analyses section for an evaluation of how the vulnerability calculations are affected by the specification of λ. $VoCC_c$ was estimated individually for each ESM and then averaged across all ensemble models.

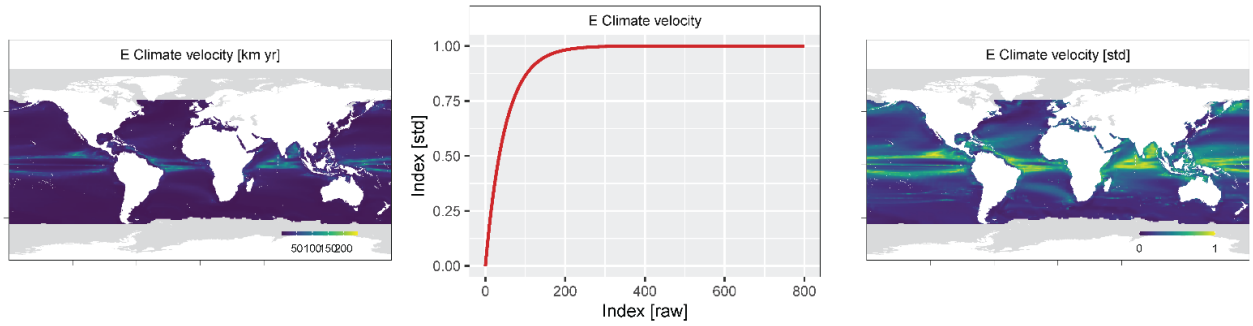

Figure S21 | Velocity of climate change for Shortfin mako.
The velocity of climate change was calculated across the native geographic distribution of shortfin mako (left panel) and transformed using the function described by Equation 11 (middle) to standardize them (right).

The transformation altered the distribution of the climate velocities to make them less skewed (Figure S22).

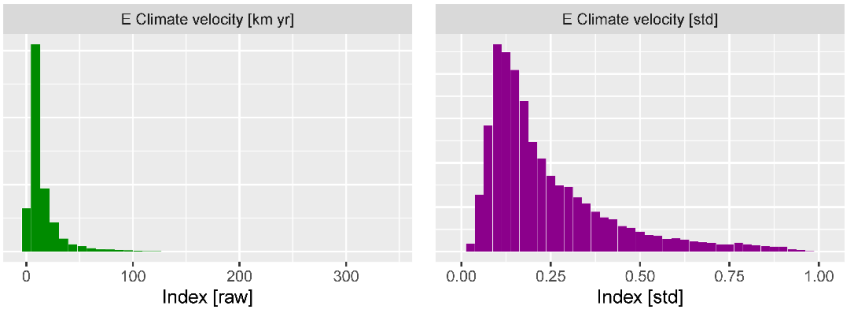

Figure S22 | Distribution of the projected climate velocities.
Histograms depict the probability distribution of projected climate velocities before (green; left) and following (purple; right) standardization.

Adaptivity to climate indices

Overview

The concept of adaptivity is analogous to the well-known concept of resilience from ecological stability theory[16]. Adaptivity describes the extent to which species can recover from perturbations. It is predominantly defined by the life-history traits of species, their native geographic distribution characteristics, and the habitat to which they have been historically exposed[*e.g.* 75].

Geographic range extent

Rationale

Geographic range extent refers to the total geographic area and latitude spanned by species. Species distributed broadly are thought to have a greater adaptivity to climate changes; there is a greater breadth of suitable climatic and habitat conditions (*e.g.* climate refugia) within their geographic distributions, buffering them against adverse climate changes[23,53,54,71,74]. Alternatively, range-restricted species are more likely to depend on specific habitat types and thus vulnerable to climate-driven habitat alteration. The latitude spanned by species is significant to their climate vulnerability, as temperature and climate change impacts have consistently varied by latitude[47,49–52]. The total geographic range area (km)[10,26,61,75] and the latitude range of species[10,57,75] are frequently used in climate vulnerability analyses to index their adaptability or sensitivity to climate change.

Calculation

An index of the adaptivity of each species was calculated as a bivariate function of the geographic range area (km^2), and latitude spanned by their native geographic distributions over the spatial domain of our CCRA analysis (*i.e.* global). The geographic range area (km^2) occupied by each species was calculated from their native geographic distribution at a global 1˚ resolution obtained from AquaMaps and standardized by the maximum global occupancy area possible for any marine species (361,900,000 km^2). Adaptivity to climate change increased exponentially with the geographic range area of each species as

$$AC\ Rarea_s = 1 - e^{-\lambda Rarea_s}, \quad \text{Equation 12}$$

where $Rarea_s$ is the geographic range area (km^2) of species *s*, and λ is the rate parameter, set at 20. The rate parameter (λ) and resulting equation were chosen to standardize the index (0-1), normalize it's distribution and specify that adaptivity increases asymptotically with geographic range area, with the greatest adaptivity occurring for species with the largest geographic range areas. The adaptivity was virtually uniformly high for species inhabiting >20% of the global ocean area (Figure S23). Refer to the Quality control and sensitivity analyses section for an evaluation of how the vulnerability calculations are affected by the specification of λ.

The latitude range of species was calculated as the difference between the highest and lowest latitude occupied by a species across its native geographic distribution obtained from AquaMaps. The ranges were standardized on a 0-1 scale by the maximum possible latitude range (90 degrees) as

$$AC\ Lrange_s = \frac{Lrange_s}{90}, \quad \text{Equation 13}$$

A standardized index of adaptivity as a function of the geographic range extent ($AC\ Grange_s$) was then calculated for each species as the mean of the standardized geographic range area ($AC\ Rarea_s$) and latitude spanned ($AC\ Lrange_s$).

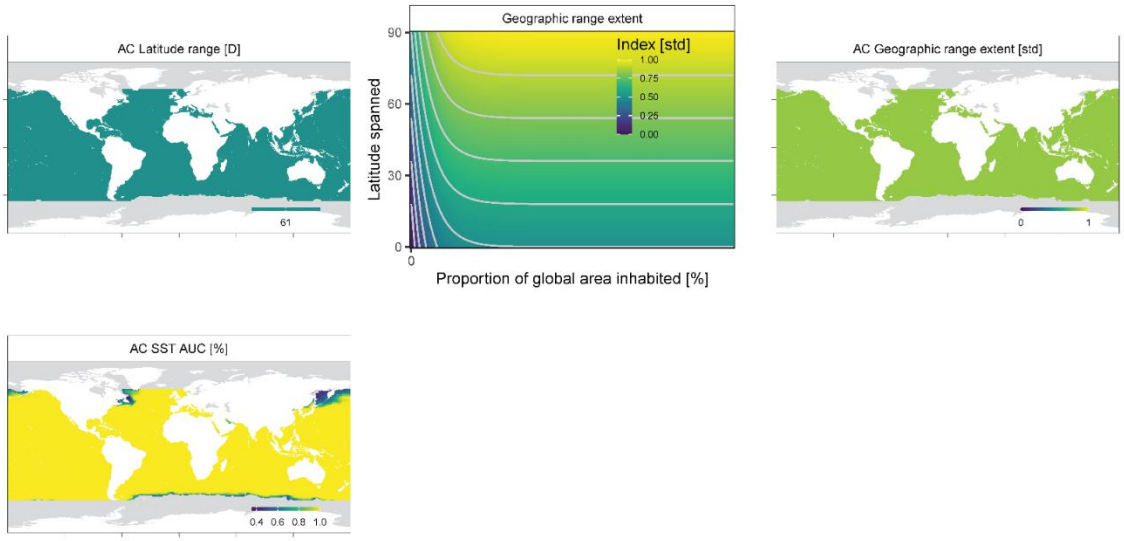

Figure S23 | Geographic range extent of Shortfin mako.
The geographic range extent of shortfin mako as a fraction of the total global ocean area (left) was transformed using the function described by Equation 12 (middle) to derive standardized values (right).

The statistical distribution of the geographic range area and latitude range of species before and after transforming them is shown in Figure S24.

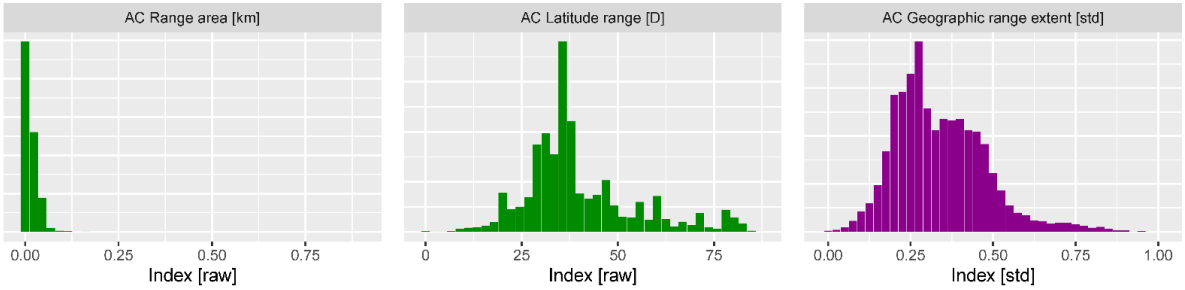

Figure S24 | Distribution of the habitat ranges of all species.
Histograms depict the probability distribution of habitat ranges for species before (green; left) and following (purple; right) standardization.

Geographic habitat fragmentation

Rationale

Range fragmentation refers to the number of distinct isolated habitat patches that a species occupies across its native geographic distribution. Species with less fragmented habitat ranges have greater access to potentially favourable habitats (*e.g.* climate refugia), migration corridors, and larval dispersal. Alternatively, habitat fragmentation increases the isolation of habitat patches reducing the probability that they can be recolonized following local extinctions (*e.g.* the 'rescue effect'[77]) and increases the amount of edge habitat in those patches. Consequently, studies in terrestrial and marine systems have reported that species with fragmented geographic ranges are more sensitive to and less resilient to climate change impacts[10,55–58,71,82], primarily by affecting their extinction and colonization[e.g. 59]. Habitat fragmentations are also known to aggravate the negative impacts of habitat loss on populations[78–81].

Calculation

The extent of geographic habitat fragmentation for each species across the spatial domain of our CCRA analysis (*i.e.* globally) was calculated from their native geographic distribution at a global 1° resolution

obtained from AquaMaps. Habitat fragmentation was calculated from the number of patches in a species native distribution standardized by its total geographic distribution area. The number of patches was estimated using landscape analysis methods[133,134] as

$$NP_s = n_i, \qquad \text{Equation 14}$$

where n_i is the number of patches in the species native geographic range, where patches must be connected in eight directions (queen's case=8 cells surrounding). NP was standardized to density by the total number of grid cells in the present-day species range. A standardized habitat fragmentation index was then calculated as

$$AC\ Hfrag_s = e^{-\lambda Hfrag_s}, \qquad \text{Equation 15}$$

where $Hfrag_s$ is the geographic habitat fragmentation of species *s*, and λ is the rate parameter, set to 8. The rate parameter (λ) and resulting equation were chosen to standardize the index (0-1), normalize it's distribution and specify that adaptivity due to habitat fragmentation declines asymptotically with geographic range fragmentation, with the lowest adaptivity occurring for species with highly fragmented habitats (Figure S25). The adaptivity was virtually uniformly low for species with >25% of their present-day distribution fragmented. Habitat fragmentation calculations were made in the R statistical computing platform using the *landscapemetrics* package[134]. Refer to the Quality control and sensitivity analyses section for an evaluation of how the vulnerability calculations are affected by the specification of λ.

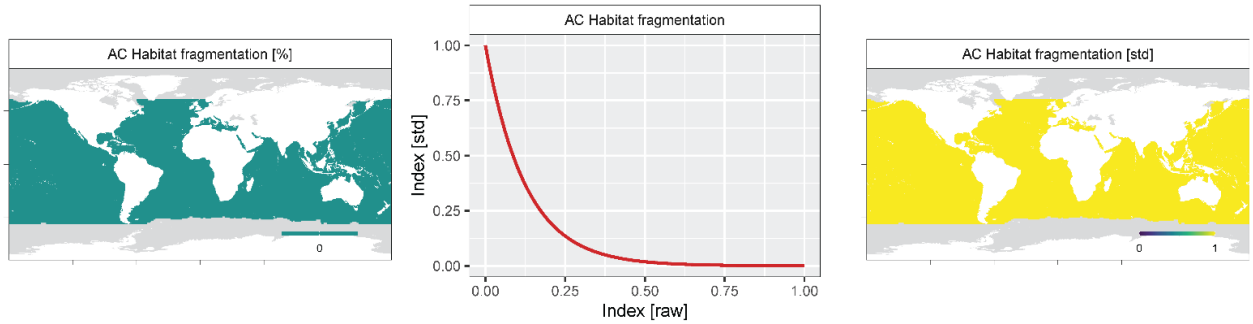

Figure S25 | Habitat fragmentation of Shortfin mako.
The habitat fragmentation of shortfin mako (left) was transformed using the exponential function described by Equation 15 (middle) to derive standardized values (right). Habitat fragmentation was calculated as the number of habitat patches in a species native geographic distribution standardized by its entire distribution area. Species with a greater concentration of fragments (patches) in their distribution have a lower adaptivity.

The distribution of species' habitat fragmentation is shown in Figure S26.

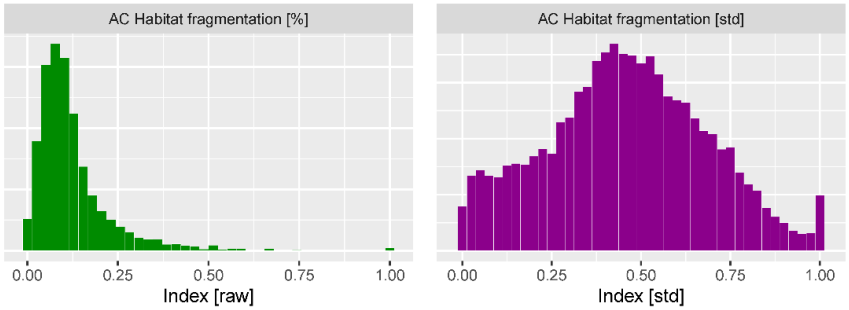

Figure S26 | Distribution of the habitat fragmentation of all species.
Histograms depict the probability distribution of the habitat fragmentation of species (green; left) and following (purple; right) standardization.

Thermal habitat variability and use

Rationale

Ecological disturbance theory suggests that species and ecosystems that experience high natural variability are more adapted to cope with climate change[86]; empirical analyses have supported this theory[87,135]. Similarly, species inhabiting more variable thermal environments such as at the range-edges of their geographic distributions are thought to have a greater capacity to adapt to climate change[65–67] and are believed to be less sensitive to it[10]. Continued exposure to temperatures close to the species' thermal preferences is thought to 'stretch' their thermal niche and pre-adapt them to temperatures outside of their thermal preferences. Through this mechanism, species can exhibit different levels of plasticity in their thermal sensitivity depending on the variability in their thermal environment[68].

Calculation

We developed an index that quantifies the proportion of the total available thermal habitat each species has inhabited over the past 40 years (1981-2021) in relation to its thermal preference range. Forty years was used as a pre-adaptation duration because it is the minimum baseline over which high-resolution ($4km^2$) remote sensing observations of surface temperature are available. The temperatures experienced by species in the past 40 years were obtained from the NOAA 0.25° daily Optimum Interpolation Sea Surface Temperature dataset (OISST) between 1981 and 2021. The dataset combines observations from different observation platforms (satellites, ships, buoys, and Argo floats). For each 1° grid cell, a count of the frequency of SST values in each 1°C bin was obtained; each temperature distribution (Tdist) characterizes the range and frequency of historical temperature within each 1° cell. For each species within each 1° cell across its native geographic distribution, the area under the Tdist curve within the species temperature preferences (red shading in Figure S27) was standardized by the total area under the Tdist curve (gray + red shading in Figure S27).

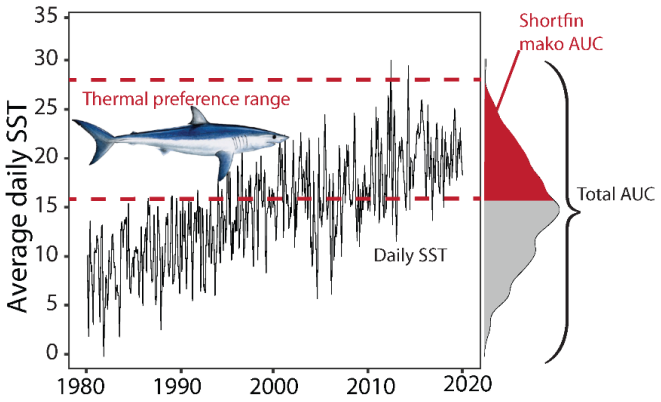

Figure S27 | Adaptivity of species calculated from their thermal habitat variability and use.
The adaptivity of a species was defined by the frequency to which it is exposed to temperatures at the extremes of its thermal preference range. Frequency of exposure to extreme temperatures was defined as the ratio of the area under the curve (AUC) of the total available thermal habitat (black line and gray shaded density), that is within the shortfin mako thermal preference range (red dashed lines and red shaded density). Species that are more frequently exposed to temperatures at their temperature preference extremes are assumed to have a higher adaptivity.

A standardized index was then calculated as

$$AC\ TAUC_s = \frac{e^{\lambda TAUC_s}}{e^{\lambda}}, \qquad \text{Equation 16}$$

where $TAUC_s$ is the proportion of the total thermal habitat within the thermal niche of species *s*, and λ is the rate parameter, set to 4. The rate parameter (λ) and resulting equation were chosen to standardize the index (0-1), normalize its distribution and specify that adaptivity due to thermal habitat pre-adaptation increases exponentially with the proportion of the thermal habitat occupied (Figure S28). The resulting index characterizes the proportion of time that a species inhabits temperatures close to its thermal preference range. Species that inhabit a greater proportion of their total potential thermal habitat are, theoretically, more pre-adapted to climate change than those that inhabit less. Refer to the Quality control and sensitivity analyses section for an evaluation of how the vulnerability calculations are affected by the specification of λ.

The variability of the thermal environment experienced by a species is another crucial characteristic of pre-adaptation. Species inhabiting more thermally variable environments are believed to have a higher adaptivity to any thermal environment changes. Accordingly, each species' temperature variability was calculated as the total temperature range (maximum-minimum) within each grid cell across its native geographic distribution over the previous 40 years (1981-2021; Figure S28).

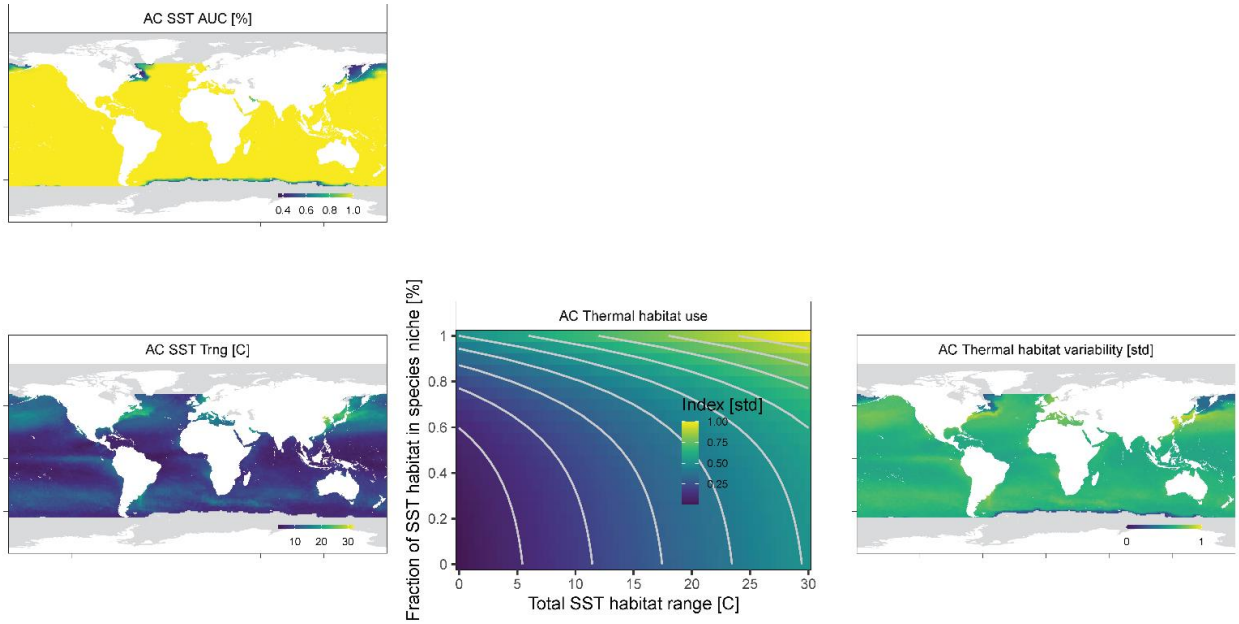

Figure S28 | Thermal habitat variability and use for Shortfin mako.
The total SST habitat variability across its geographic distribution and fraction of the time the SST habitat is within the species' (left) defines the thermal habitat variability index (middle and right). Species inhabiting more thermally variable habitats at the extremes of their thermal preferences have higher adaptive capacities (yellow area in middle plot).

The distribution of the thermal habitat use and variability indices for species before and after transforming them is shown in Figure S29.

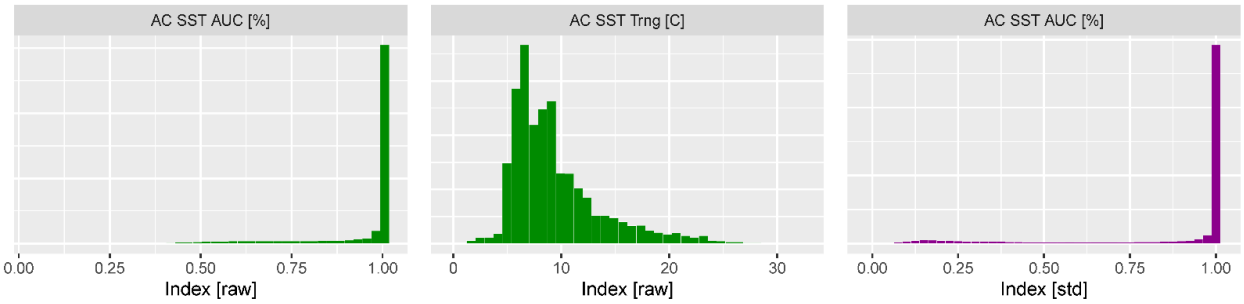

Figure S29 | Distribution of the thermal habitat variability and use of all species.
Histograms depict the probability distribution of the thermal habitat use (green; left), thermal habitat variability (green; middle), and standardized thermal habitat use index (purple; right) for all marine species.

Maximum body length

Rationale

The maximum size (length or mass) reached by species has been commonly used as a proxy of extinction risks, susceptibility to exploitation, and species vulnerability to climate change[4,10,57,60–62,75,83]. The maximum size is a predictor of several life-history traits (*e.g.* generation length, time to maturity, intrinsic rate of population increase) that cumulatively define species' potential reproductive capacity and population growth rate (Figure S30)[63,64,75,83,84]. Ecologically, body size has been used to classify species as *r*- (produce many offspring, high growth rates and mortality) or *K*-selected (produce fewer offspring, low growth rates and mortality). For these reasons, the maximum body length was used as an indicator of species' resilience or adaptivity to the potential adverse effects of climate change (Figure S30), whereby smaller species that grow

and reproduce faster have a higher adaptivity[4,10,57,60–62,71,75,83]. The maximum body length of species (cm) was estimated from the FishBase[3] and SeaLifeBase[4] databases (see Data compilation section).

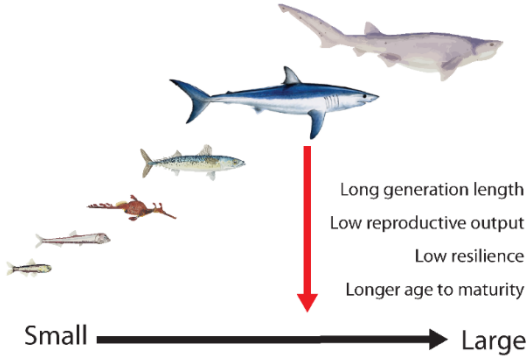

Figure S30 | Maximum body size represents species' adaptivity.
The maximum body size of species is related to several of their reproductive attributes. Larger species are generally less resilient to perturbations and thus have a lower adaptivity.

Calculation

A standardized index of adaptivity as a function of the maximum possible body length of each species was calculated as

$$AC\ Mlen_s = 1 - MlenSTD_s, \qquad \text{Equation 17}$$

where $MlenSTD_s$ is calculated as

$$MlenSTD_s = \frac{log10(Mlen_s+1)}{log10(3000+1)}, \qquad \text{Equation 18}$$

$Mlen_s$ is the maximum estimated length of species *s* (cm), and 3000 is a scaling factor corresponding to the approximate maximum length that the largest oceanic species (*i.e.* blue whale) could conceivably reach. The equation was chosen to normalize and standardize the index (0-1). Through this approach, much of the change in adaptivity occurred for changes in maximum body length between 0 and 100 cm (0-3.3ft), which seems biologically plausible considering the dramatic differences that exist in population doubling time between the smallest plankton (days) to fish that can reach 100 cm (*e.g.* Shortfin mako; ~2-4yrs). The equations predict that a species' adaptivity declines asymptotically with its maximum possible length, with the lowest adaptivity occurring for species with larger body sizes that have slower growth rates and population doubling times and lower mortality rates. The most rapid changes in $AC\ Mlen_s$ occur for small-bodied species, such as those with body lengths between 0 and 5 m and decline more moderately thereafter (Figure S31).

[3] http://www.fishbase.org
[4] https://www.sealifebase.ca/

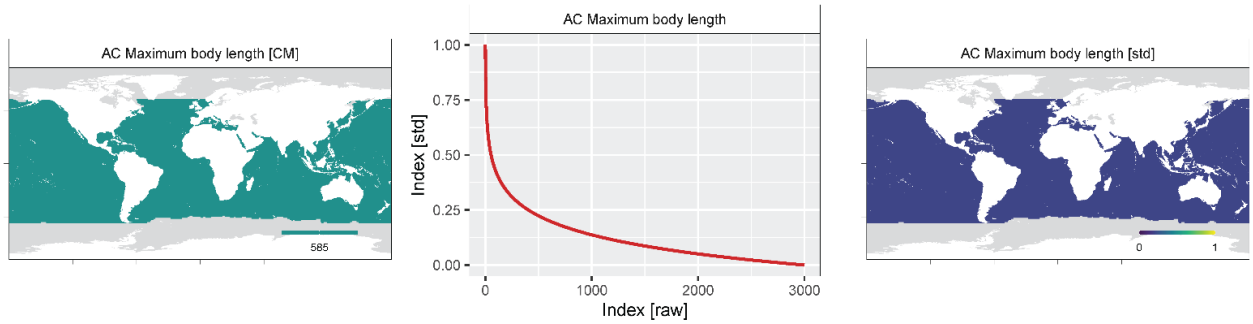

Figure S31 | Adaptivity defined by maximum body size for Shortfin mako.
The maximum body size for shortfin mako (left) was transformed using the function described by Equation 18 (middle) to standardize it (right).

The distribution of the maximum body lengths of species before and after transforming them is shown in Figure S32.

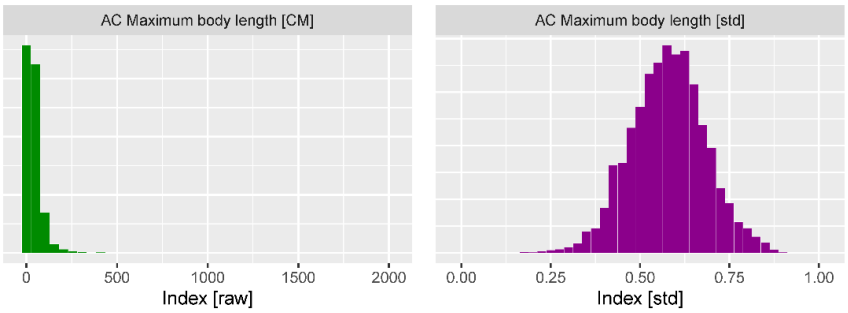

Figure S32 | Distribution of the maximum body lengths of all species.
Histograms depict the probability distribution of the maximum body lengths of species before (green; left) and following (purple; right) standardization.

4. Calculating climate vulnerability

The 12 climate indices were used to calculate vulnerability and its dimensions two ways: (1) for each species, at all locations across their geographic distributions (taxonomic and spatial), (2) for each species, averaged across their geographic distributions (taxonomic).

Species across their geographic distributions

For each species within each grid cell across its native geographic distribution, the sensitivity, exposure, and adaptivity were calculated as the average of the four indices that define them. The standard deviation of the vulnerability dimensions provided an estimate of their statistical uncertainty and was propagated forward through all subsequent vulnerability calculations using variance weighting (read below).

Because the sensitivity analyses suggested that the omission of any of the 12 climate indices in any grid cell could affect the vulnerability scores (Figure S33), the analysis was restricted to cells containing all 12 indices. Conversely, the sensitivity analyses suggested that the vulnerability scores for species were relatively insensitive to missing values across their geographic distributions; guided by this result, it was determined that species could have upwards of 10% of grid cells across their native geographic distribution missing with minimal effect on the resulting vulnerability scores.

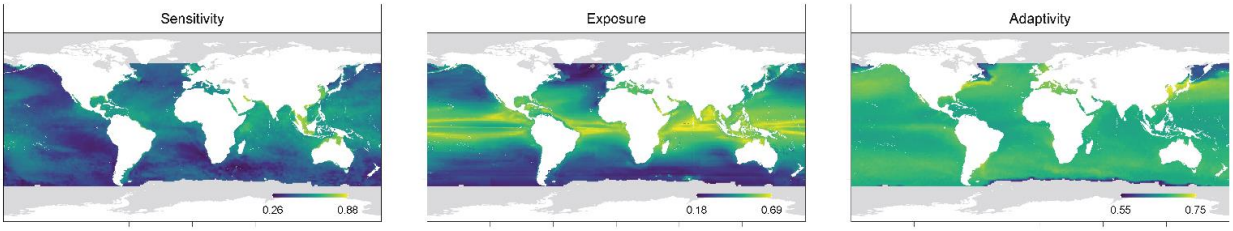

Figure S33 | Dimensions of vulnerability for Shortfin mako.
The sensitivity (left), exposure (middle) and adaptivity (right) of Shortfin mako are calculated from the 12 indices across its native geographic distribution.

For each species, s, and grid cell, c, across their native geographic distribution, vulnerability ($V_{s,c}$) was calculated from sensitivity, exposure, and adaptivity, while statistically accounting for both their variability and the statistical uncertainty associated with the indices of climate exposure calculated from ensemble climate projections.

First, we statistically accounted for the uncertainty associated with the model-projected climate exposure of species through discounting. Discounting is common in economics and was used to develop the ocean health index (OHI) to account for the greater uncertainty associated with unknown future states[32]. Its use in the vulnerability estimation is analogous: the future exposure of species to climate change, estimated from ESM projections, are less well resolved than are their sensitivities or adaptive capacities, which are primarily based on the current and historical conditions, respectively. Our confidence in the reliability of the projected exposure indices scales with the length of the climate projection and the number of ensemble projections. Accordingly, these factors define a discount rate ∂. With all else being equal, exposure indices derived from single ESMs that make longer-term climate projections are less reliable[51,136–138] and are thus more heavily discounted. Those derived from a larger ensemble of ESMs that make shorter-term projections are perceived as more reliable and are discounted less. The discount rate was calculated as

$$\partial = \frac{Years}{100\theta} + \frac{Models}{-20\theta} + \vartheta, \qquad \text{Equation 19}$$

Where $Years$ is the number of years in the climate projection, $Models$ is the number of climate projections in the ensemble, θ is a scaling factor set to 40, and ϑ is 0.026 to yield a maximum discount rate of 5% when projections are made for >=100 years from a single projection and are 0% when projections are made for <5 years from >19 projections. Our study evaluated climate projections from 12 models over 80 years, yielding a discount rate of 3.1%. To conserve the vulnerability scaling to between zero and one, discounts applied to exposure are credited to sensitivity, such that the maximum total adjustment is 10%.

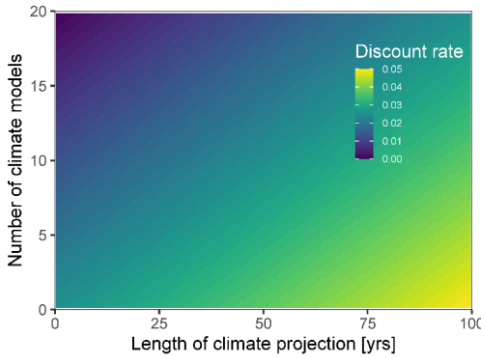

Figure S34 | Discount rates.
The discount rate on future exposure, credited to the present state, is a function of the length of the climate projection(s) and the size of the climate ensemble. Future conditions that are more uncertain due to far-future projections from a few ESMs are discounted more (5%) relative to those that project over the near future from many models (0%).

For each species within each grid cell across its native geographic distribution, the discount rate was applied to the estimated exposure and sensitivity as

$$\breve{E}_{s,c} = [(1 - \partial)(E_{s,c})]\,, \qquad \text{Equation 20}$$

$$\breve{S}_{s,c} = [(1 + \partial)(S_{s.c})]\,, \qquad \text{Equation 21}$$

Where $\breve{S}_{s,c}$ and $\breve{E}_{s,c}$ are the discounted sensitivity and exposure estimates for species s within cell c. Through this equation, the future exposure of species to climate change was discounted relative to their current sensitivity. The discounting was applied to sensitivity, rather than adaptivity, as there is a broad consensus that it is better understood[e.g. 139]. Following this procedure, vulnerability was calculated as a weighted average of adaptivity and discounted sensitivity and exposure as

$$V_{s,c} = \frac{\left[\breve{S}_{s,c} \times \omega S_{s,c}\right] + \left[\breve{E}_{s,c} \times \omega E_{s,c}\right] + \left[\left(1 - AC_{s,c}\right) \times \omega AC_{s,c}\right]}{\omega S_{s,c} + \omega E_{s,c} + \omega AC_{s,c}} \qquad \text{Equation 22}$$

where $V_{s,c}$ is the vulnerability, $\breve{S}_{s,c}$ and $\breve{E}_{s,c}$ are the discounted sensitivity and exposure, respectively, and $AC_{s,c}$ is adaptivity for species s within cell c. $\omega S_{s,c}, \omega E_{s,c}$, and $\omega AC_{s,c}$ are the statistical reliability weights for the estimated sensitivity, exposure, and adaptivity, calculated from their scaled variances. For example, the weights for estimated sensitivities were calculated as the inverse of their coefficients of variation as

$$\omega S_{s,c} = \left(\frac{\sigma S_{s,c}}{\mu S_{s,c}}\right)^{-1} \qquad \text{Equation 23}$$

where

$$\mu S_{s,c} = \frac{1}{n}\sum_{i=1}^{n} S_{s,c,i} \qquad \text{Equation 24}$$

and

$$\sigma S_{s,c} = \sqrt{\frac{\sum_{i=1}^{n}\left(S_{s,c,i} - \mu S_{s,c}\right)^2}{NS_{s,c}}} \quad \text{Equation 25}$$

where $\omega S_{s,c}$ is the reliability weight and $\sigma S_{s,c}$ and $\mu S_{s,c}$ are the standard deviation and mean, respectively, of the four indices, i, that define sensitivity for species s within cell c. $NS_{s,c}$ is the number of climate indices, i, that define sensitivity for species s within cell c. This process estimated climate vulnerability for each species across the totality of its geographic distribution (Figure S35).

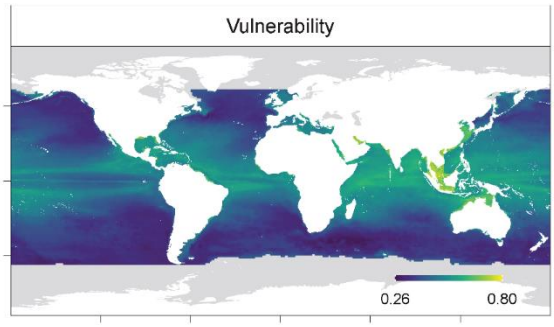

Figure S35 | Geographic patterns of climate vulnerability for Shortfin mako.
The vulnerability of Shortfin mako across its native geographic distribution was calculated from the 12 indices using Equation 22.

Species

For each species, s, we calculated vulnerability and its variability while statistically accounting for geographic differences in its uncertainty using inverse variance-weighting. The vulnerability for each species was calculated as a variance-weighted mean of the vulnerabilities in each grid cell across its geographic distribution as

$$V_s = \frac{\sum_{c=1}^{n} \omega V_{s,c}\, V_{s,c}}{\sum_{c=1}^{n} \omega V_{s,c}} \quad \text{Equation 26}$$

while their variance-weighted standard deviations were calculated as

$$\sigma V_s = \sqrt{\frac{v_1}{{v_1}^2 - v_2} \sum_{c=1}^{N} \omega V_{s,c} (V_{s,c} - \mu V_{s,c})^2} \quad \text{Equation 27}$$

where,

$$V_1 = \sum_{c=1}^{N} \omega V_{s,c} \quad \text{Equation 28}$$

and

$$V_2 = \sum_{c=1}^{N} {\omega V_{s,c}}^2 \quad \text{Equation 29}$$

and

$$\omega V_{s,c} = \left(\frac{\sigma V_{s,c}}{\mu V_{s,c}}\right)^{-1}, \quad \text{Equation 30}$$

In this manner, a greater statistical weighting is given to vulnerability estimates in grid cells where their variance (*e.g.,* variance across the indices used to calculate them) is lower and vice-versa. Species vulnerability estimates will be more variable when the vulnerability is more dissimilar in the grid cells that comprise its geographic distribution and vice-versa.

5. Calculating climate risk

Climate change vulnerability has been almost exclusively reported in dimensionless units, allowing species and ecosystems to be scored and ranked on relative, but not absolute, scales. This approach helps to understand patterns and trends in species climate vulnerabilities *relative to the other species assessed within the same vulnerability analysis.* Yet, such relative vulnerability scores can tell us little about the absolute climate risks of species that are often needed in management and policy settings. For instance, regional assessments often rank species by their relative vulnerabilities against each other but rarely address the overarching question that managers and stakeholders are interested in: how many and which species are at high climate risk, and where are they most at risk? Indeed, interpreting the meaning of vulnerability rankings in dimensionless units on relative scales has been a significant challenge. It may be a contributing factor for their low incorporation into management. Previous vulnerability studies, or the comparably holistic cumulative impact index, have defined categories of high/low according to the statistical distribution of the dimensionless indices that represent them[4,10,31,95]. Here, we instead define climate risk thresholds that enable climate vulnerability to be translated into categories of risk according to the ecological interpretation of each of the 12 climate indices. Despite the challenges in reliably defining such risk thresholds[140], they are increasingly being used to help guide conservation strategies and actions[74,141–143]. The risk thresholds are defined in their native units and propagated through the analysis, preserving their meaning and interpretation yet informing the interpretation of the dimensionless vulnerability scores. This approach is comparable to the definition of extinction risk used by the IUCN Red List of species[69], the definition of safe operating space in planetary boundaries theory[144], and the reasons for concern (RFC) framework adopted to define climate risk by the Intergovernmental Panel on Climate Change (IPCC)[7,145,146]. It allows the vulnerability of species and communities to be categorized according to our ecological interpretation of them and is guided by, rather than defined by, their statistical properties. Defining thresholds to define risk is notoriously challenging[140,147] due to various factors, including a lack of knowledge needed to define them, uncertainties in climate model projections, and differences in value judgments regarding what constitutes dangerous risk[140,147–150]. However, threshold-defined risk assessments have proven immeasurably valuable in helping to communicate risks to a broad audience while supporting public engagement, management, and policy decisions.

For instance, since 2001, the IPCC RFC framework has communicated levels of climate risk to humans using thresholds set by expert judgement[*e.g.* 146]. The resulting ‘burning embers’ diagrams have become widely used tools to communicate the risks stemming from anthropogenic climate change in a clear, intuitive manner that is critical for decision-making[147]. For instance, the goal of the Paris Agreement to limit

global warming to below 2°C was supported by IPCC reports of increasing risks beyond 1.5°C or 2°C warming[148,149]. It is, however, essential to define risk thresholds using transparent and, where possible, empirically supported approaches[151–153]. The following describes our rationale for defining a midpoint threshold (TH_M) to denote high/low climate risk, as well as the lower (TH_L) and upper (TH_U) thresholds that denote critical and negligible risk categories, respectively. These thresholds represent waypoints to guide the definition and communication of climate risk. To the extent possible, they were guided by empirical information. Nonetheless, some thresholds were unavoidably defined using less objective criteria. We anticipate that some of these thresholds may be refined as our knowledge of ecological thresholds continues to improve. The risk thresholds and their rationale and associated references are listed in

Table S4.

Sensitivity

TH_M of thermal safety margins was set at 2ºC, TH_L at 1ºC and TH_U at 5ºC. These values were guided by observed and projected rates of surface warming. For example, TH_M of 2ºC is comparable to the warmest surface warming rates globally over the past century[52], whereas 5ºC compares to projected warming to 2100[154].

Since the vast majority of IUCN Red Listed species were classified as 'least concern, this category was adopted as a natural threshold for both TH_M and TH_L. TH_U was set at 'vulnerable,' with all species classified within or above this classification defined as very high sensitivity.

Thresholds for sensitivity by cumulative impacts were guided by the categories presented in Halpern *et al.* [31] and by the upper and lower 10% quantiles of its distribution. TH_M was set at 1.4, the level defined in Halpern *et al.* [31] as their low/very low impact threshold. TH_U was set at 2 (90th percentile), while TH_L was set at 0.6 (10th percentile).

Thresholds for vertical habitat use were set individually for the maximum depth of occupancy and vertical habitat range. TH_M, TH_U and TH_L by maximum depth were set at 100, 50, and 200m, respectively. By these thresholds, sensitivity is high within the upper 100m, where warming is greatest, and only becomes very low at depths exceeding the epipelagic zone (200m).

These climate sensitivity risk thresholds were propagated through the analyses described previously, enabling the relative sensitivity scores to be translated into absolute sensitivity risk categories (Figure S36).

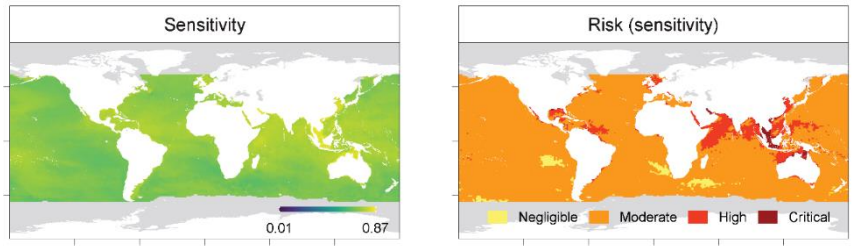

Figure S36 | Climate sensitivity and risk for Shortfin mako.
The relative sensitivity of Shortfin mako across its native geographic distribution (left) translated into absolute risk categories (right).

Exposure

The projected time of climate emergence is a newly developed index of the timing of climate change exposure of species, and thus, there are not yet objective guidelines to define risk. We set TH_M, TH_L and

TH_U by projected ensemble time of thermal niche emergence at 50, 75, and 25 years, respectively. These thresholds were, to an extent, guided by the IUCN RedList categories and criteria for listing. Under the RedList criteria for a listing of vulnerable under Criterion E, species must have a 10% chance of extinction within 100 years[69]. Assuming that the instantaneous probability of local species extinction is a function of the death rate (*d*), our TH_U of 25 years would yield a *d* of $138x10^{-5}$; following this, our TH_M and TH_L values (50 and 75 years) would then yield extinction probabilities of 7% and 3% respectively by 2116 (100 years). Therefore, exposure to hazardous climate by 2040 (TH_U of 25 years) is very likely to lead to at least a 10% chance of extinction under a RedList assessment criterion of vulnerable.

Although the loss in thermally suitable habitat has been used in climate vulnerability studies[95], there were few objective thresholds to define risk from it in marine systems. However, modelling studies and reviews suggest that the maximum permissible habitat loss threshold for species is 10-50%[155,156], comparable to estimates of minimum habitat required for species persistence estimated in freshwater[157] or terrestrial[143,158] systems. Following this, TH_M, TH_L and TH_U by projected ensemble change in suitable thermal habitat of species were set at 10, 5, and 20%, respectively.

TH_M, TH_L and TH_U by the projected fraction of species lost due to warming were set at 10%, 5%, and 20%, respectively. There is considerable uncertainty regarding the safe operating space for ecosystems and of species loss therein[159–162]. However, our thresholds were guided by meta-analytic studies that have suggested a 20% loss of species as one possible threshold[38,161,163].

TH_M, TH_L and TH_U by projected ensemble climate velocity were set at 15, 6, and 30 km yr^{-1}, respectively. Lacking a clear basis for their ecological interpretation, these thresholds were set by the 50^{th}, 10^{th}, and 90^{th} quantiles of the distribution of global velocity values.

These climate exposure risk thresholds were propagated through the standardization analyses described previously, enabling the relative exposure scores to be translated into absolute exposure risk categories (Figure S37).

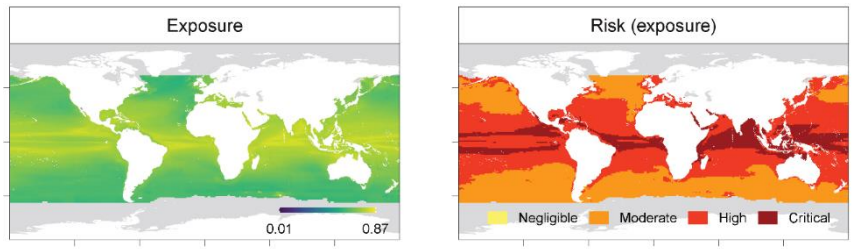

Figure S37 | Translation of climate exposure to climate risk for Shortfin mako.
The relative exposure of Shortfin mako across its native geographic distribution (left) translated into absolute risk categories (right).

Adaptivity

Thresholds of adaptivity defined by maximum species body size were referenced by the relationship between maximum body size and the intrinsic rate of population increase, which is linear on a log-log scale. TH_L adaptivity was set when the change in intrinsic population increase becomes negligible (100cm), and

TH_U was set where its change becomes rapid (10cm). TH_M, denoting the high/low adaptivity threshold, was set at 30cm, the point at which the intrinsic rate of population increase was moderate; this threshold was also the median of all body lengths in our database (Figure 39).

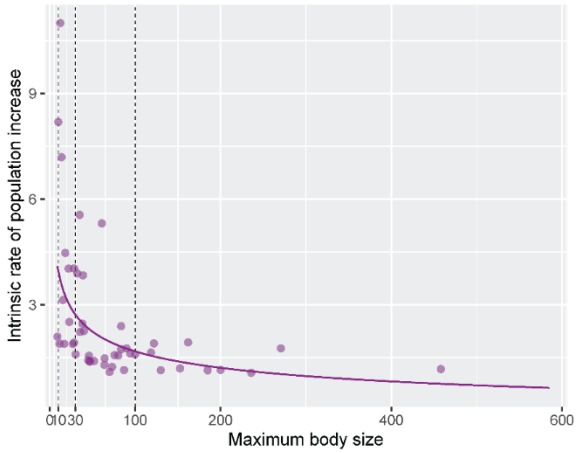

Figure S38 | Maximum body size of species in relation to their intrinsic rate of population increase.
Points show the maximum body size (cm) versus the intrinsic rate of population increase for 51 species within FishBase and SeaLifeBase. The line is the best fitting log-log linear regression model fitted to the data (r^2=0.59; p<0.0001). Vertical lines are the thresholds denoting very low (10cm), midpoint (30cm) and very high (100cm) adaptivity.

Thresholds for adaptivity defined by geographic range extent were set individually for the total geographic area and latitude spanned. Thresholds of adaptivity defined by geographic range extent were referenced to the size of large marine ecosystems (LMEs)[164]. TH_U of range extent vulnerability was defined by the size of the largest large marine ecosystems (LME; Arabian Sea=3.84M km^2=1% of the global area), TH_M by the median area of all LMEs (1.2M km^2=~4% of the global area) and TH_L by the size of the smallest LME (Faroe Plateau=151,005km^2=0.04% of the global ocean).

TH_M, TH_U and TH_L by latitude spanned were set at 45°, 60°, and 20°, respectively. These values approximate the latitude span of marine biogeographic provinces (*e.g.* tropical, temperate, polar) that have been identified from analyses of large scale climatological (*e.g.* winds), oceanographic (*e.g.* mixing, currents, nutrient availability), and ecological (*e.g.* primary production) features[*e.g.* 165–167].

TH_M of adaptivity as defined by habitat fragmentation was set at 10%, TH_U at 20% and TH_L at 1%. These values are comparable to those defined for the vulnerability of marine mammals, except our midpoint threshold is slightly higher (10%) than that defined by Albouy *et al.* [10]; (2-4%).

Thresholds for thermal habitat variability were set individually for the total temperature range and proportion of available thermal habitat occupied by the species across its geographic range. TH_M, TH_U and TH_L sensitivity by temperature range were set at 15°, 5°, and 10°C, respectively. TH_M of temperature range is identical to that used to define the vulnerability of marine mammals according to thermal habitat range [10]. TH_M, TH_U and TH_L adaptivity by thermal habitat occupancy was set at 95%, 99%, and 80%, respectively.

These climate adaptivity risk thresholds were propagated through the standardization analyses described previously, enabling the relative adaptivity scores to be translated into absolute adaptivity risk categories (Figure S39).

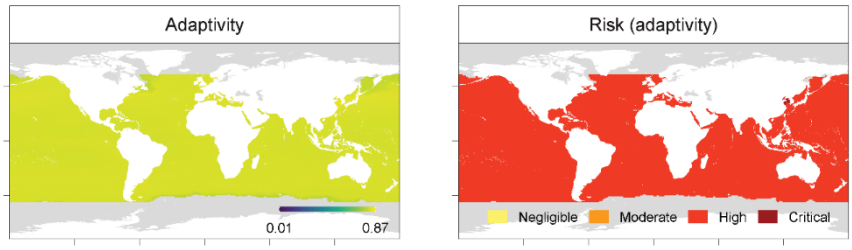

Figure S39 | Translation of climate adaptivity to climate risk for Shortfin mako.
The relative adaptivity of Shortfin mako across its native geographic distribution (left) translated into absolute risk categories (right).

The climate thresholds were propagated through the analyses using the equations described previously (Calculation of the indices), thus enabling climate vulnerability scores to be translated into absolute risk categories (Figure S40).

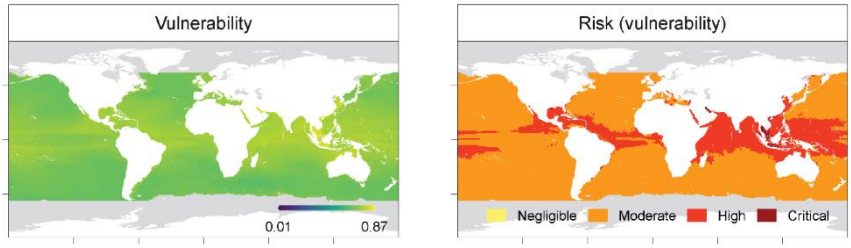

Figure S40 | Translation of climate vulnerability to climate risk for Shortfin mako.
The relative climate vulnerability of Shortfin mako across its native geographic range (left) translated into absolute risk categories (right).

Table S4 | Thresholds used to define climate risk categories.

Dimension	Index	Tlow	Tmed	Thigh	Rationale	References
Sensitivity	Thermal safety margin	5°C	2°C	1°C	Guided by warming rates. 1°C and 2°C compare to the rates of Warming over the past 50, 100 years, respectively[52]. 5° to projected warming [154].	[20,21,52,72,168]
Sensitivity	Conservation status	LC	LC	V, E, CR	Defined by the IUCN RedList categories and criteria[69]: any category at or above 'vulnerable' is considered at high risk.	[69]
Sensitivity	Cumulative impacts	0.6	1.4	2	Guided by [31].	[31,73]
Sensitivity	Vertical habitat variability and use					
Sensitivity	Maximum depth	200m	50m	20m	Standard pelagic biogeochemical divisions within the euphotic zone to categorize variation in *e.g.* mixing, nutrients, photosynthetically active radiation, primary production.	
Sensitivity	Vertical range	200m	50m	20m	Standard biogeochemical divisions within the euphotic zone to categorize variation in *e.g.* mixing, nutrients, photosynthetically active radiation, primary production.	
Exposure	Projected climate velocity	6km yr^{-1}	15km yr^{-1}	30km yr^{-1}	Guided by the quantiles of the statistical distribution.	
Exposure	Projected time of climate emergence from the thermal niche	75yrs	50yrs	25yrs	Guided by the IUCN RedList assessment criteria[69].	[38,69]
Exposure	Projected loss of suitable thermal habitat	5%	10%	20%	Guided by [143,155–158].	[94,142,143,155–158,169–171].
Exposure	Projected ecosystem disruption	5%	10%	20%	Guided by thresholds in [38,161,163].	[38,76,142,159,161–163]

Adaptivity	Geographic range extent					
Adaptivity	Latitude span	20°	45°	60°	Based on oceanographic and ecological domains that vary by latitude and are defined by biogeographic patterns in *e.g.* seasonality, ocean circulation, climate[165–167]	[165–167,169]
Adaptivity	Total geographic area	0.04%	1%	4%	Referenced to the size spectrum of large marine ecosystems[164].	[54,76,143,155–157,164,169–171]
Adaptivity	Geographic habitat fragmentation	20%	10%	1%	Guided by and comparable to those defined in [10] for the vulnerability of cetaceans.	[10,76,79,80,143,158,169,171–173]
Adaptivity	Maximum body length	100cm	30cm	10cm	Empirically guided by the relationship with the intrinsic rate of population increase.	[63,84,85]
Adaptivity	Thermal habitat variability and use					
Adaptivity	Thermal habitat occupancy	8%	95%	99%	Guided by the quantiles of the statistical distributions	[65,67]
Adaptivity	Thermal habitat variability	5°C	10°C	15°C	Comparable to those defined in [10] for the vulnerability of cetaceans.	[10,65–67,86,89]

6. Quality control and sensitivity analyses

Criteria for species inclusion

Species that did not inhabit the upper 100m of the ocean (*e.g.* their depth range did not encompass the upper 100m) were excluded from the analyses, as were those whose maximum depth of occurrence exceeded 1000m, as surface temperatures could weakly define the vulnerability of these species. To validate this threshold, we evaluated the relationships between surface temperatures (SSTs) and temperatures at increasing depths (Figure S41). The monthly averaged temperatures at depths used for this sensitivity analysis were obtained from the 2018 National Oceanographic Data Center World Ocean Atlas[NODC WOA; ,174]. The SSTs and coincident temperatures at depths within the upper 200m were positively correlated for all months (r=0.92-0.97), and the SSTs well approximated the temperature variations across depths (absolute difference ~3°C).

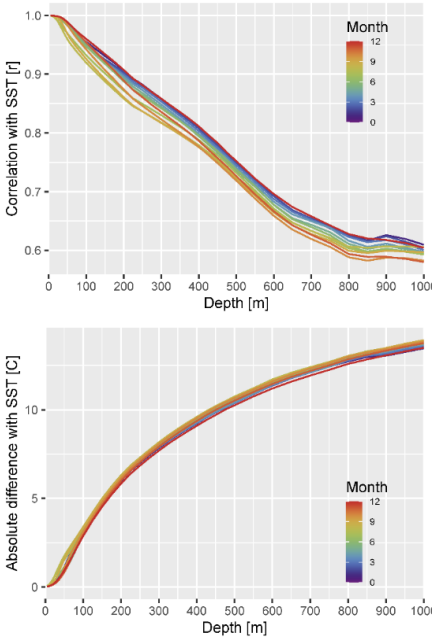

Figure S41 | Relationships between spatial gradients in global ocean temperatures at the surface and across depths.
The relationships (top) and absolute differences (bottom) between spatial gradient in SSTs and the corresponding temperatures at increasing depths are shown. Colours show the months of the temperature observations.

Thresholds of acceptable index missingness

We evaluated the sensitivity of the sensitivity, exposure, adaptivity, and vulnerability to the 12 input climate indices' absences. From a random sample of 5000 species that contained complete observations (12 indices present across their native geographic distributions), we simulated all 4,016 possible combinations of index missingness (range=3 to 11 indices present). For each scenario (n=4,016), the difference between the sensitivity, exposure, adaptivity, and vulnerability calculated using the complete database was compared against each simulation for each species. This approach allowed us to quantitatively determine the effect of the number of indices omitted and the missing index identity on the estimates of vulnerability and its dimensions. It also enabled us to identify indices associated with a high sensitivity level whose omission had disproportionate effects on vulnerability and its dimensions.

Overall, the vulnerability calculations were relatively insensitive to missing indices (Figure S42). The omission of any single index led to an average change in the vulnerability of 6% relative to complete sampling. Omitting half of the indices (n=6) resulted in an average change in the vulnerability of 20% relative to complete sampling. However, we found that missing indices had a larger impact on the derivation of the climate dimensions. The omission of a single index resulted in an average change in sensitivity, exposure, or adaptivity of between 20 and 23% but could be as high as 63%, with three out of four indices missing.

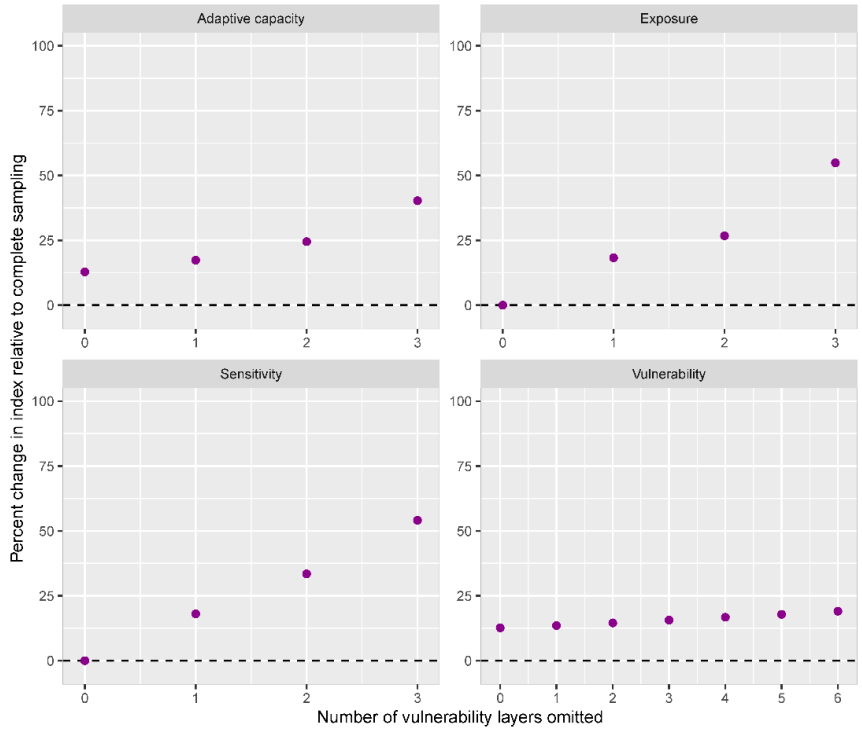

Figure S42 | Effect of missing indices on the calculation of climate dimensions and of vulnerability.
Points show the estimated differences between (*y-axes*; %) the climate dimensions and of vulnerability calculated across the entire range of species under different simulated levels of index missingness (*x-axes*). Each point was calculated from every conceivable combination of indices containing the specified level of missingness, across 5000 species (total: 4,016 possible missingness patterns). Vertical lines about the points depict the 95% confidence intervals about the means.

Thresholds of acceptable data spatial missingness

We evaluated the effect of missing observations across species' native geographic distribution on the climate indices through simulation analyses. From a sample of 5,396 species that contained complete observations across their predicted native geographic distributions, we randomly sampled each vulnerability index under different scenarios of data completeness (range=40%-100%; n=19 levels). This random sampling was repeated 50 times for each species, generating 5,126,200 simulations (5,396 species, 19 missingness levels, 50 replicates per species) for each of the 12 climate indices. For each simulation, we calculated the difference between each vulnerability index across each species distribution with complete sampling (no missing observations) and with the simulated data missingness level; differences were expressed as percentage change, relative to 'true' value, *i.e.* that calculated with complete sampling. The average difference was calculated across the 50 simulations for each species and vulnerability index. Lastly, we estimated the average effect of data missingness and its variability on each vulnerability index across all species using linear models. The effect of data missingness on the calculation of the vulnerability index varied but was generally small (Figure S43). When averaged across all species, a missingness level of 60% (40% data coverage) resulted in a change in the climate indices of 1%-2%. At 20% missingness (80% data coverage) the climate indices changed 0.4%-0.8% and at 10% missingness (90% coverage) they changed 0.3%-0.5%.

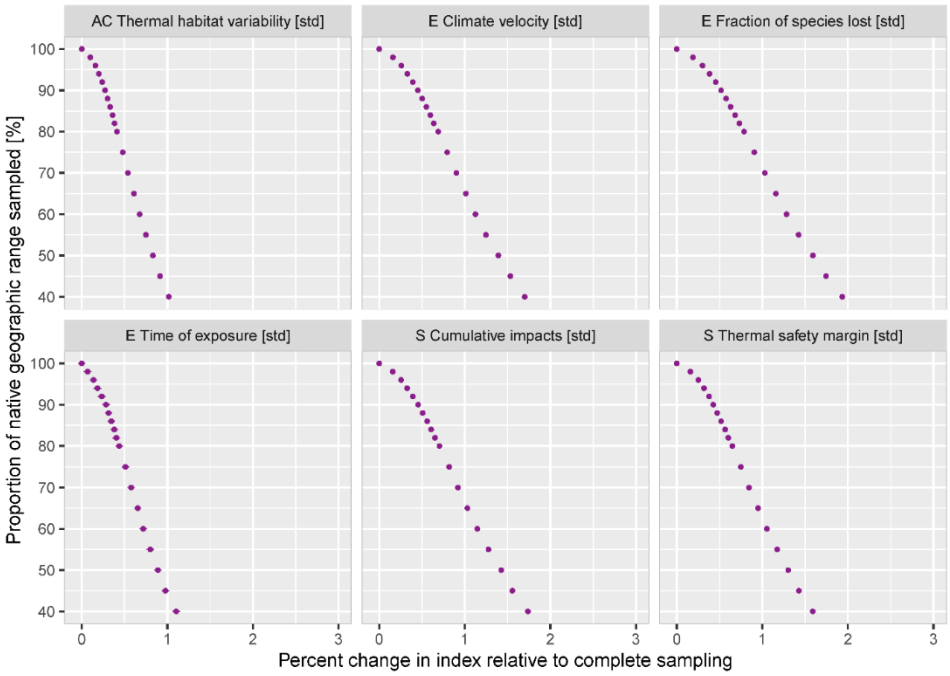

Figure S43 | Effect of missing observations across species' native geographic distribution on the calculation of climate indices.
Points show the estimated differences between the climate indices calculated across the entire range of species and those calculated under different simulated levels of missingness (y-axes). Each point was calculated from 20 replicated missingness patterns and estimated across all species for which complete data exists (n=5,396). Horizontal lines about the points depict the 95% confidence intervals about the means. Analyses were undertaken for the 6 climate indices that exhibit spatial variation.

The sensitivity of the analyses to the transformation functions

It was not possible to objectively derive the transformation functions that standardized the climate indices. In many instances, standard transformations, such as log10, led to normalized and standardized indices but did not have ecological meaning. Instead, the transformation functions were chosen to ensure that the climate indices were ecologically grounded and were rooted in our understanding of how climate vulnerability scales with species traits, human stressors, ecosystem dynamics, and environmental change. The transformations were secondarily chosen to standardize the indices between 0 and 1 and reduce extreme skewness in their distributions, making them more susceptible to statistical outliers. However, because each index's transformation function was derived subjectively, we also conducted sensitivity analyses to gauge their efficacy. Specifically, we quantitatively evaluated the impact of alternative transformation functions on the calculation of vulnerability, its indices and dimensions under different levels of observation missingness. We evaluated the impact of several transformations (Figure S44): i) untransformed (raw) but standardized between 0-1, ii) the transformations used in the analysis, iii) the transformations used in the analysis with the parameters scaled by factors of 2, iv) 3, v) 5, and vi) 10. For each transformation, the indices were individually rescaled (range=0-1) to ensure that they were compared in the same standardized units (% of the maximum). For each alternative transformation (n=6), we calculated the 12 indices, the vulnerability dimensions, and vulnerability accordingly for each of 1000 species across their native geographic distribution. We then compared the vulnerability and its dimensions for each species under these different transformations to gauge the sensitivity of the vulnerability estimation to our chosen transformation. This

approach does not determine the correct transformation but instead informs us of the overall sensitivity of the vulnerability calculations to standardization.

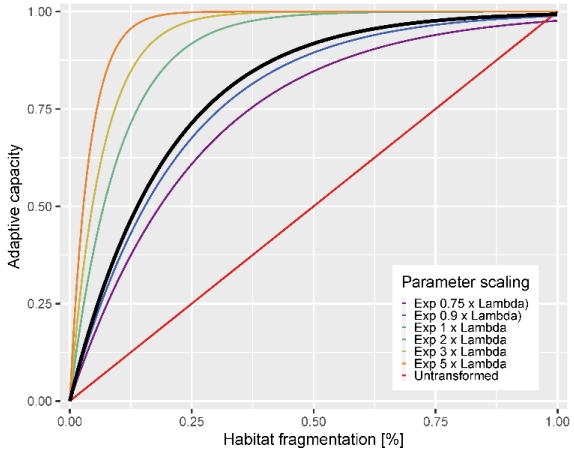

Figure S44 | Alternative transformation functions tested.
Different transformation functions used to standardize climate indices are shown. Colours depict the exponential transformation parameter scaling employed and black is the parameter used in our study. Red=unstandardized.

Relative to the transformation parameters used in our study ($\lambda = 1$), using no transformation ($\lambda = 0$), led to an average relative difference in species vulnerability scores of 2%, while scaling up the parameters by a factor of 2 (*e.g.* doubling; $\lambda = 2$) led to an average relative difference in the vulnerability of 8% (Figure S45). The effect of changing the transformation parameters on calculated sensitivity and adaptivity to climate changes were comparable to vulnerability. Relative to the parameters used in our study, using no transformation led to an average relative difference in species adaptivity scores of 9% while scaling up the parameters by a factor of 2 led to an average relative of 4%. Relative to the parameters used in our study, using no transformation scaling led to an average relative difference in species sensitivity scores of 8%, while scaling up the parameters by a factor of 2 led to an average relative difference of 2%. Lastly, relative to the parameters used in our study, using no transformation scaling led to an average relative difference in species exposure scores of 7%, while scaling up the parameters by a factor of 2 (*e.g.* doubling) led to an average relative difference of 26%.

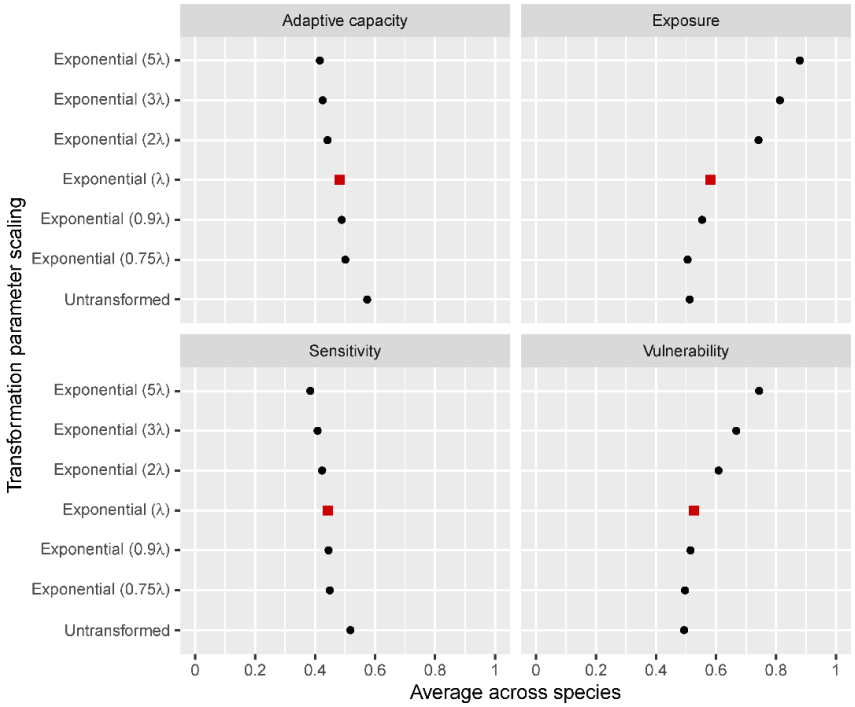

Figure S45 | Average vulnerability of species calculated under the different transformation functions shown in Figure S44.
Points show the average vulnerability score across all species calculated from climate indices standardized using the exponential parameters shown in Figure S44. The red point denotes the transformations used in our study.

In our study, species' vulnerability scores remained positively correlated to those calculated using alternative transformation parameters (r=0.75-1; Figure S46).

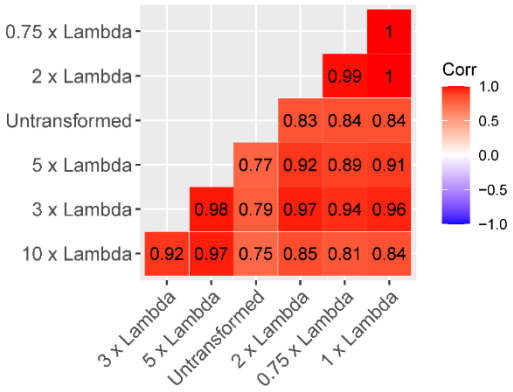

Figure S46 | Correlations between species vulnerability scores estimated in our analysis against those calculated under the different transformation functions shown in Figure S44.

The transformation functions that standardized the climate indices could affect the species relative vulnerability scores. However, as the risk thresholds used to define risk are propagated through the same transformations, the risk assessments are less sensitive to the choice of transformation parameters. Overall, these analyses suggest that the vulnerability calculations are relatively insensitive to the transformation functions relative to untransformed data or the magnitude of the parameters used to derive them.

Missing data

Body length estimates or IUCN Red List assessments were available for 8,865 and 6,455 of the 24,938 assessed species, respectively; they were, however, unavailable or data deficient for many species. The sensitivity analyses we undertook (see Thresholds of acceptable index missingness section) indicated that omission of these or any of the 12 climate indices could potentially bias the vulnerability estimates. To maximize the number of species for which vulnerability could be evaluated, we gap-filled missing body lengths and Red List extinction risk values using the approaches described below.

Imputation of body lengths

We estimated missing body lengths multivariate imputation by chained equations (MICE). MICE is an increasingly common and recognized approach for dealing with diverse types of missing data (*e.g.* continuous or binary) and has previously been used to gap-fill missing observations in vulnerability studies[9]. Using MICE, missing values are imputed based on the observed values for a given variable and the relationships observed in the data for other associated variables. An ensemble of imputations is estimated for each missing value, and these are used to produce correct standard errors for the imputations. Imputing missing values has resulted in significantly less bias in subsequent analyses relative to case-wise deletion [175].

Simulation analyses were undertaken to provide confidence in the imputation routine and to produce valid estimates. 5,415 species contained observations of body length. We randomly sampled body length observations from this species pool to simulate varying levels of missing-ness: 50%, 60%, 70%, 80% and 90%. For each random draw of varying sampling intensity, we estimated the missing values using MICE using different imputation methods: classification and regression trees, random forests, a random sample from observed value, proportional odds model, and linear discriminant analysis. Predictive variables for the imputation included minimum and maximum species tolerance values (temperature, oxygen, net primary production, salinity, ice concentration, distance from land, and depth of occupancy), latitude range, geographic distribution, and taxonomy (phylum, order, family). The five most probable imputations and their ensemble average were retained. We evaluated the correlation between the true lengths and the imputed and the relative difference between them for continuous body length values. This procedure allowed us to evaluate the effectiveness of MICE to successfully gap-fill missing body lengths values under different levels of missingness and imputation approaches. Ensemble averaging the top five most probable imputations led to a better prediction of the true values relative to the single most probable imputation. The imputation was relatively insensitive to the proportion of missing values that were imputed (range 50-90% missing). Imputation of missing values via random forests was the optimal approach. Ensemble averaging the top 5 imputations yielded body length estimates that were positively correlated to the true values under all levels of missingness (r=0.5-0.61). With a missingness level of 60% (missingness in our analysis=~65%), the correlation between imputed and estimated body lengths was 0.56). The agreement between the imputed and actual body length values increased when evaluated on a log-log scale, consistent with their vulnerability analysis treatment (see Maximum body lengths section).

Gap-filling of Red List statuses

We explored the feasibility of imputing missing Red List (RL) extinction risk values using the MICE approach described above for body lengths. For the categorical Red List extinction categories, we evaluated the proportion of imputed values that were correctly classified. Imputation via proportional odds models slightly outperformed the other methods and correctly classified assessment status 94% of the time, on average (Figure S47). However, the average classification accuracy of the imputation diminished when moving from species of least concern (LC; 99%) to those that were threatened or near-threatened, vulnerable, or critically endangered (~30%).

Given these results, we considered two possible approaches to gap-fill missing RL statuses: (1) imputing missing RL values with the understanding that the classification accuracy will likely be more uncertain for non-LC species (*e.g.* a higher type II error rate). Under this approach, we accept the possibility of incorrectly estimating the status for ~7% of the missing species in our analysis, representing ~4% of all species. (2) Uniformly assigning the highest probability outcome (status=LC) for each missing RL value (*e.g.* a higher type I error rate). With this approach, we accept the certainty of underestimating the status for ~6% of missing species but understand the type of error that we are imposing (*e.g.* higher type I error rate). After weighing the pros and cons of each approach carefully, we opted to uniformly assign an LC status to all missing or data deficient RL values. This approach to gap-filling offers several advantages over the imputation of missing values. First, this approach is the most conservative, as species with unknown RL statuses will have lower overall climate risk than may be the case. Second, in assigning LC values uniformly, there is a clear, unambiguous understanding that we are avoiding type II errors (which we feel are possibly more problematic) at the expense of a higher type I error rate. Lastly, forgoing imputation simplifies the analysis and makes it more reproducible and accessible.

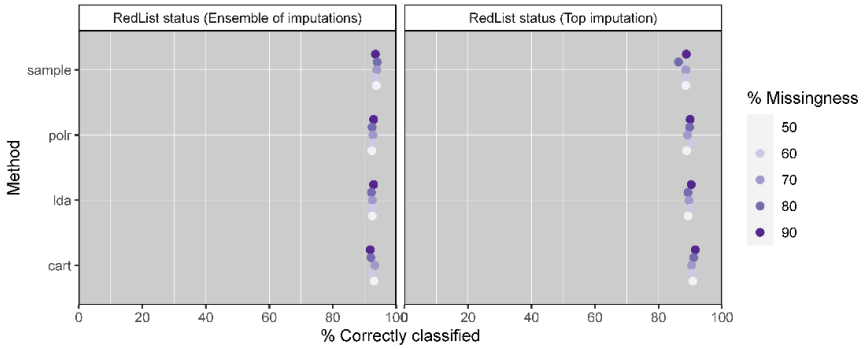

Figure S47 Estimation of missing Red List assessment status of species.
Points are the average proportion of correctly classified species into Red List assessment categories under different simulated missingness levels and multivariate imputation methods. Colours depict the extent of simulated data missingness (range 50-90%). The ensembles of the top 5 imputations (left panel) and most probable imputations (right panel) are shown. Methods: polr=proportional odds model, lda=linear discriminant analysis, cart=conditional autoregressive model.

Defining species native geographic distribution

Species presences were inferred from their probabilities of occurrence estimated from AquaMaps and ranged from 0 (no occurrence) to 1 (certainty of occurrence). Ideally, species native geographic distribution would be defined as the probability of occurrence significantly different from 0. However, as the probability

of occurrence lacked statistical uncertainty estimates, this approach was unfeasible, and we needed to define probability thresholds for species presences. Previous studies using AquaMaps native geographic distributions have used probability thresholds ranging from those greater than 0[176] to greater than 0.5[177,178]. Rather than arbitrarily setting a probability threshold, we conducted our analyses under three contrasting occurrence thresholds: i) >0, ii) >0.25, and iii) >0.5. We then evaluated the effect of the probability threshold on the estimation of climate vulnerability and risk across all species and ecosystems. Increasing the threshold from 0 to 0.5 yielded species vulnerability and risk scores that were broadly similar (r=0.95; average vulnerability difference=4.4%; Figure S48). Varying the occurrence threshold has a minimal effect on the species vulnerability rankings (Figure S49). In general, increasing the probability threshold from 0 to 0.5 led to higher species and ecosystem vulnerability and risk for 66% of species; 82% under the high emissions scenario and 51% under low emissions. The higher risk with increasing probability threshold primarily resulted from the lower adaptivity due to the reduced species habitat range and higher fragmentation; the sensitivity and exposure scores were relatively insensitive. Increasing the probability threshold from 0 to 0.5 led to different risk outcomes for 10% of species (7% under high emissions and 13 under low). Given these results, and our desire to produce conservative estimates of climate vulnerability and risk across the totality of a species potential geographic distribution, we used a probability of occurrence threshold of >0. We wanted to ensure that our analysis minimized the chance of type II errors (*e.g.* error of omission), whereby parts of a species realized geographic distribution were omitted. Hence, even though species realized distribution might be smaller than the estimated native distribution in our analysis, it is nonetheless contained within it.

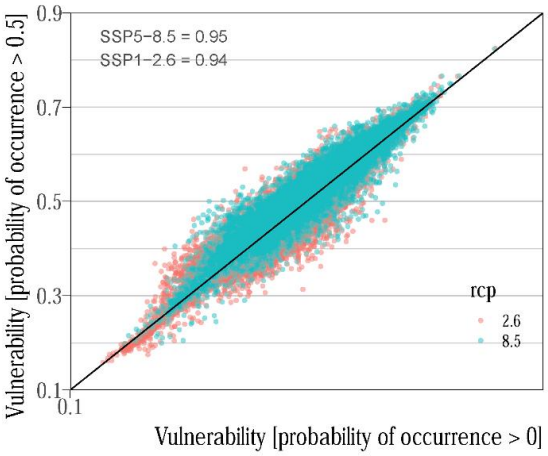

Figure S48 Relationships between species vulnerability scores under contrasting probability of occurrence thresholds.
Colours depict the emission scenario.

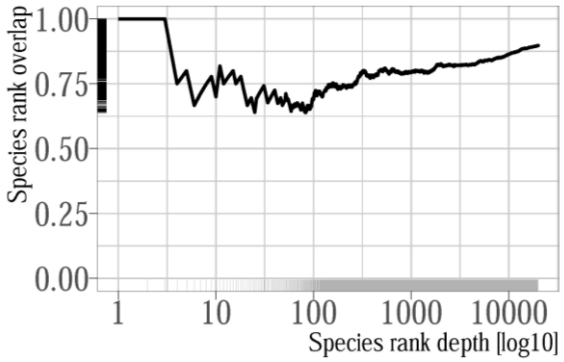

Figure S49 Average vulnerability rank similarity of species under contrasting probability of occurrence threshold.
Lines are the average overlap of species rankings when using a probability of occurrence threshold of 0.5 relative to 0. Large values denote higher ranking similarity and 0 denotes no similarity.

Collinearity of climate indices

We prioritized indices that contained unique information about species' climate vulnerability. The unique information content of the indices was quantified by calculating the variance inflation factor (VIF) between the species' climate vulnerability and all 12 climate indices[179]. VIF assessed the amount of multicollinearity in a set of multiple regression variables and is equivalent to the ratio of the total model variance to the variance of a model that includes every single predictor. VIF values above five have high collinearity. The VIF analysis suggested low collinearity among the 12 climate indices: 6 indices had extremely low scores (VIF<2), while only the projected time of climate emergence from the thermal niche has a moderately high but still acceptable score (VIF=4.3). The low VIF scores and generally weak relationships among the climate indices (Extended Data Figure 2) indicated a lack of collinearity among the climate indices.

Vulnerability across the ecosystem

We evaluated variation in climate vulnerability and risk across species' trophic levels (TLs) in all grid cells in the global ocean where the ecosystem spanned >1 TL. However, not all grid cells contained the same number and consistency of species, and hence the trophic levels spanned varied spatially. Whereas virtually all cells contained top predator species (TL>4), far less contained primary producers (TL=1) or zooplankton (TL=2-2.5). This discrepancy could be due to a lower sampling level of plankton species, as the data sources we used (*e.g.*, AquaMaps, FishBase, and SeaLifeBase) are less focussed on plankton species. For instance, grid cells in nearshore waters tended to contain more low trophic species (TL<2.5) than those in the open ocean. This variation could potentially bias the analysis. Hence, we undertook sensitivity analyses to determine if this variation affected the TL to vulnerability relationships. We fit the linear models relating the climate vulnerability of species to their TLs in each grid cell using all available data (TLs 1-5; Figure S50 top), omitting primary producer species (TLs=1; n=303 species; Figure S50 middle), and omitting primary producers and zooplankton (TLs<2.5; n=1,129 species; Figure S50 bottom). This sensitivity analysis indicated that the variation in species climate vulnerability with increasing TL was relatively insensitive to the presence or absence of low trophic level species. The proportion of all grid cells with positive regression slopes (β_{TL}>0), denoting more vulnerable high TL species, was 81% when considering all species, 82%

when omitting primary producers, and 84% when omitting all plankton; the proportions were 86%, 88%, and 96%, respectively, when considering only statistically significant trends ($p<0.05$). Under the low emission scenario, the proportion of all grid cells with positive regression parameters ($\beta_{TL}>0$), was 76% when considering all species, 76% when omitting primary producers, and 84% when omitting all plankton; the proportions were 79%, 82%, and 95%, respectively, when considering only statistically significant trends ($p<0.05$).

As an additional sensitivity check, we fit an alternative model of species climate vulnerability as a discrete binary function of their TL; under this model, low TL species were the control (TL<4) and high TL species the treatment (TL>=4). This model evaluates the difference in climate vulnerability of high TL species (*e.g.* top predators) relative to all other species in the food web and is less sensitive to data values at the extreme ends of the TL spectrum (*e.g.* low TL species). Under this alternative model and under the high emission scenario, the proportion of all grid cells with positive regression parameters ($\beta_{TL}>$), denoting more vulnerable top predator species, was 80% when considering all species, 81% when omitting primary producers, and 80% when omitting all plankton; the proportions were 91%, 91%, and 91%, respectively, when considering only statistically significant trends ($p<0.05$). Under the high emission scenario, the proportion of all grid cells with positive regression parameters ($\beta_{TL}>0$), was 71% when considering all species, 72% when omitting primary producers, and 71% when omitting all plankton; the proportions were 79%, 80%, and 79%, respectively, when considering only statistically significant trends ($p<0.05$).

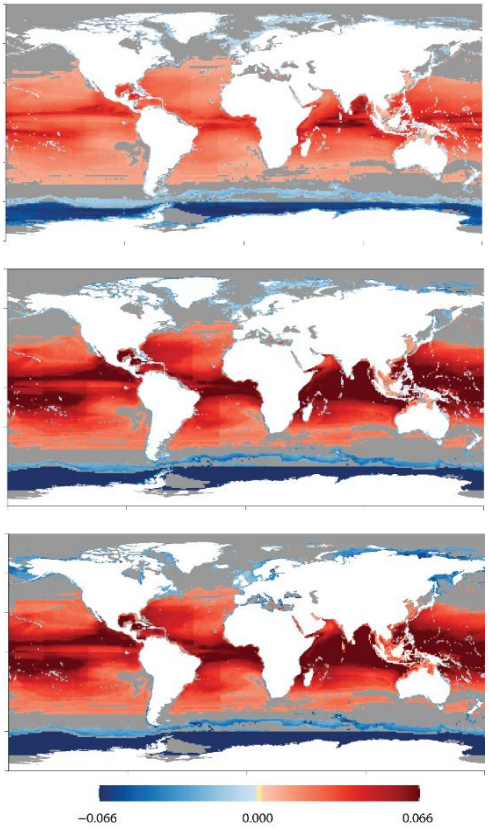

Figure S50 Relationships between trophic level and climate vulnerability.
Colours depict the magnitudes and directions of the estimated linear model slope (β_{TL}) of species' climate vulnerability by their trophic level. β_{TL} captures systematic differences between species' vulnerability given their position in the food web: red are areas where climate vulnerability increases with trophic level (e.g., top predators are most vulnerable) and blue where it declines (e.g., primary producers are most vulnerable). Gray denotes areas where data are insufficient for analyses or slopes that were non-significant (p>0.05). Slopes were calculated for all TLs (1-5; top), excluding phytoplankton (TLs 2-5; middle) and excluding zooplankton (TLs 2.5-5; bottom)

Finally, we evaluated the possibility that a possible high correlation between species maximum body lengths (which are used in the calculation of climate vulnerability) could bias the relationships between species climate vulnerabilities and their TLs. We tested the sensitivity of our results to the inclusion of body length in several ways. First, under each emission scenario, we re-fitted the linear models relating species' climate vulnerability by their trophic level in each grid cell but included species body length as a covariate in the models. This procedure enabled us to estimate the linear model slopes (β_{TL}) of species' climate vulnerability by their trophic level while holding the effect of species body lengths on climate vulnerability fixed. Including body length as a covariate did not appreciably change the overall results. The model slopes (β_{TL}) estimated from the two contrasting models were highly correlated (r>0.99), and the proportion of positive/negative slopes was relatively consistent. For instance, under high emissions, 62% of cells contained positive slopes (p<0.05) and including body length in the models increased this to 69% (p<0.05). As a next step, we evaluated the collinearity between body length and TL but estimating the variance inflation factor (VIF); [179] for each model containing TL and body length as covariates. The analysis suggested low VIF values for body length in all grid cells and emission scenarios (VIF<2.5), with virtually all cells having extremely low scores (VIF<1.5). Lastly, the correlation between species body lengths and

TLs was relatively weak (r=0.21; 5,686 species). Cumulatively, these sensitivity analyses suggest that body length was not driving the observed relationships between species' climate vulnerability and their TLs.

Supplementary figures

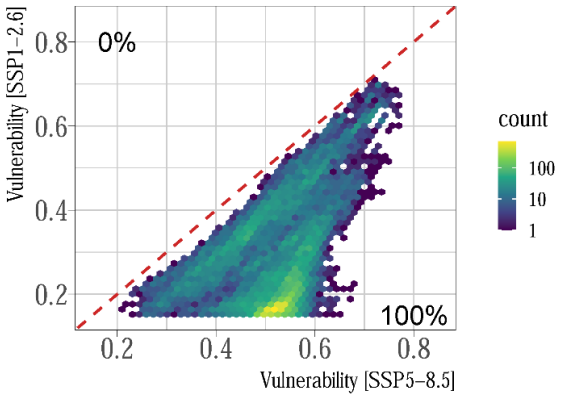

Figure S51 Average species climate exposure under different emission scenarios.

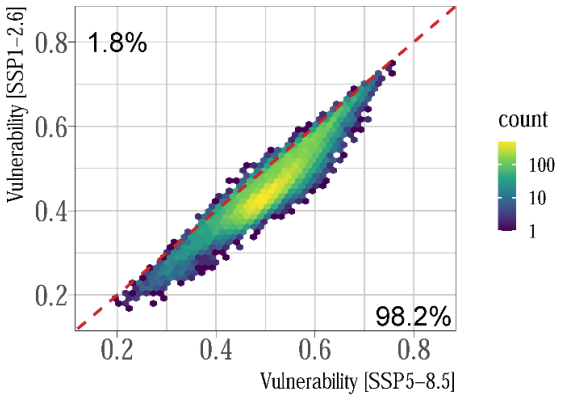

Figure S52 Average climate vulnerability of species under different emission scenarios.

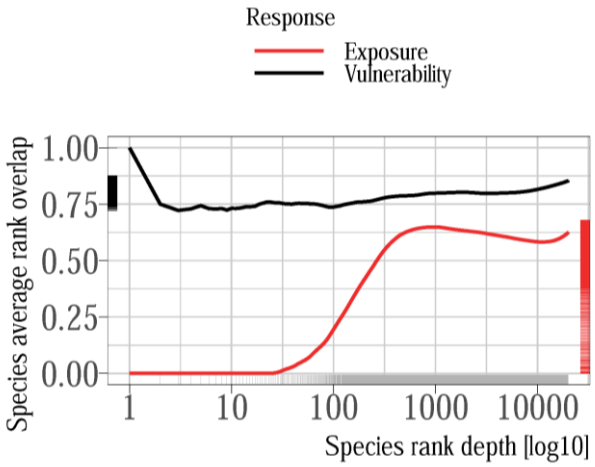

Figure S53 Average vulnerability and exposure rank similarity of species under different emission scenarios.
Lines are the average overlap of species rankings under SSP1-2.6 and SSP5-8.5 for vulnerability (black) and exposure (red). Large values denote higher ranking similarity.

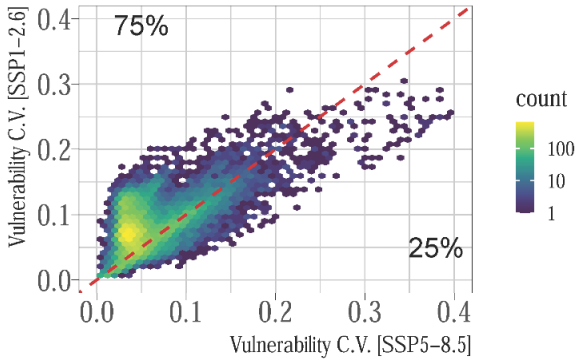

Figure S54 Average statistical uncertainty (coefficient of variation) in species vulnerability scores under different emission scenarios.

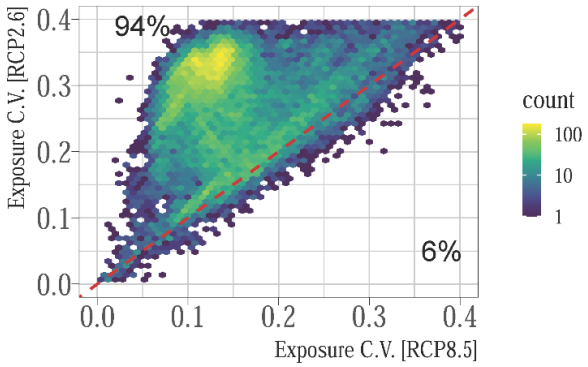

Figure S55 Average statistical uncertainty (coefficient of variation) in species exposure under different emission scenarios.

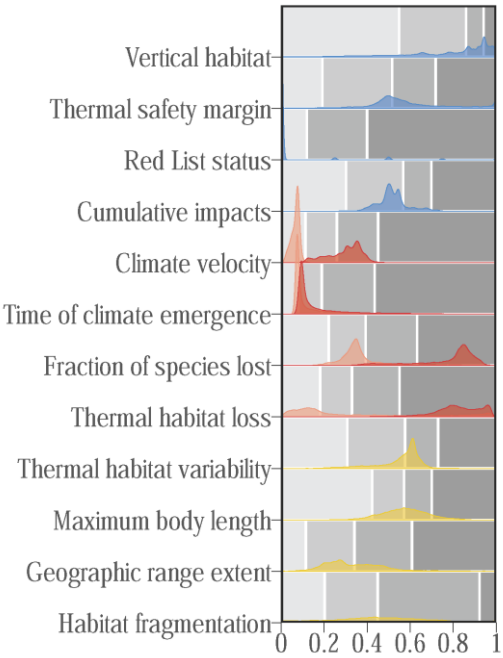

Figure S56 Statistical distribution of the 12 climate indices for all assessed species.
Coloured shading represents the smoothed numerical distributions of the species scores for the 12 climate indices in Supplementary Table 1. Colours depict the dimension: blue=sensitivity, red=exposure, yellow=adaptivity. Light red shading depicts scores under low emissions and dark red under high. Gray shading depicts the climate risk thresholds.

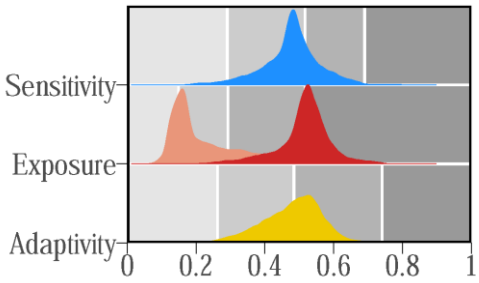

Figure S57 Statistical distribution of the 3 climate dimensions for all assessed species.

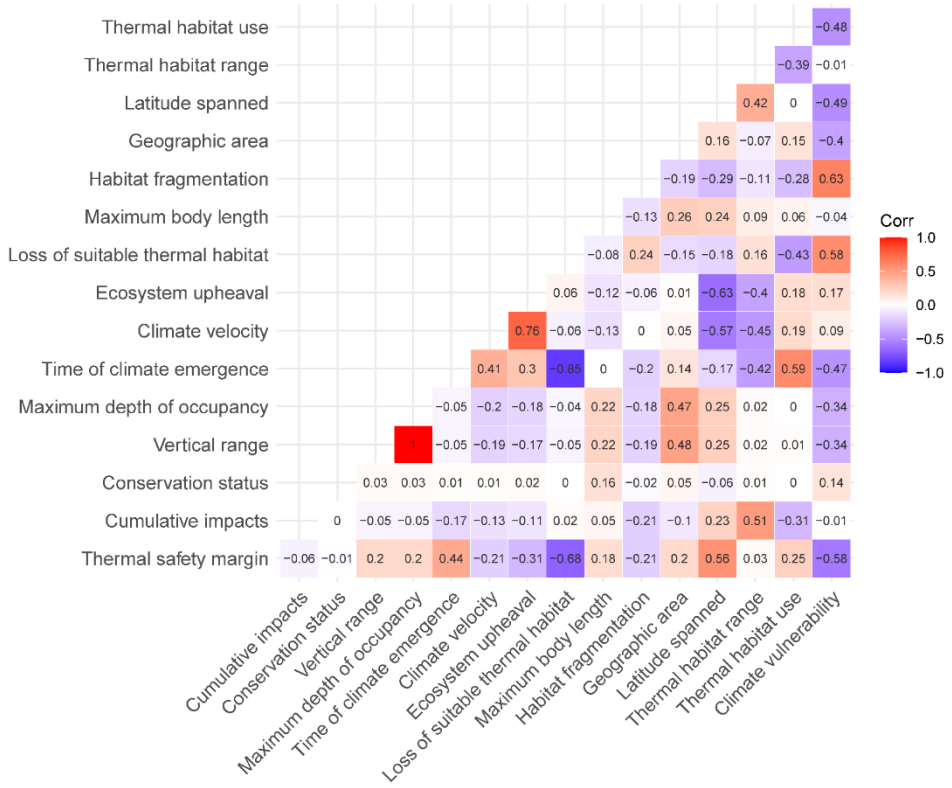

Figure S58 Correlations between species vulnerability scores estimated in our analysis against the native climate indices used to calculate it.
Colours and numbers are the correlations between climate vulnerability and the native climate indices calculated for each species. Colour shading and text are the direction and strength of the relationships: red is positive and blue negative correlations.

References

1. FAO. Impacts of climate change on fisheries and aquaculture: synthesis of current knowledge, adaptation and mitigation options. in *FAO Fisheries and Aquaculture Technical Paper* (eds. Barange, M. et al.) vol. 627 628 (2018).

2. Busch, D. S. *et al.* Climate science strategy of the US National Marine Fisheries Service. *Mar. Policy* **74**, 58–67 (2016).

3. Hare, J. A. *et al.* A vulnerability assessment of fish and invertebrates to climate change on the northeast u.s. continental shelf. *PLoS One* **11**, 1–30 (2016).

4. Foden, W. B. *et al.* Climate change vulnerability assessment of species. *Wiley Interdiscip. Rev. Clim. Chang.* **10**, 1–36 (2019).

5. de los Ríos, C., Watson, J. E. M. & Butt, N. Persistence of methodological, taxonomical, and geographical bias in assessments of species' vulnerability to climate change: A review. *Glob. Ecol. Conserv.* **15**, (2018).

6. Pacifici, M. *et al.* Assessing species vulnerability to climate change. *Nat. Clim. Chang.* **5**, 215–225 (2015).

7. IPCC. *Climate Change 2014: Impacts, Adaptation, and Vulnerability. Part A: Global and Sectoral Aspects. Contribution of Working Group II to the Fifth Assessment Report of the Intergovernmental Panel on Climate Change*. (Cambridge University Press, 2014).

8. Foden, W. B. *et al.* Identifying the World's Most Climate Change Vulnerable Species: A Systematic Trait-Based Assessment of all Birds, Amphibians and Corals. *PLoS One* **8**, e65427 (2013).

9. Comte, L. & Olden, J. D. Climatic vulnerability of the world's freshwater and marine fishes. *Nat. Clim. Chang.* **7**, 718–722 (2017).

10. Albouy, C. *et al.* Global vulnerability of marine mammals to global warming. 1–12 (2020).

11. Scheffer, M. & Carpenter, S. Catastrophic regime shifts in ecosystems: linking theory to observation. *Trends Ecol. Evol.* **18**, 648–656 (2003).

12. Scheffer, M. *et al.* Early-warning signals for critical transitions. *Nature* **461**, 53–59 (2009).

13. Scheffer, M. *et al.* Anticipating Critical Transitions. *Science (80-.).* **338**, 344–348 (2012).

14. Britten, G. L. *et al.* Predator decline leads to decreased stability in a coastal fish community. *Ecol. Lett.* **17**, 1518–1525 (2014).

15. May, R. M. *Stability and complexity in model ecosystems*. (Princeton University Press, Princeton, NJ, USA, 1973).

16. Holling, C. S. Resilience and Stability of Ecological Systems. *Annu. Rev. Ecol. Syst.* **4**, 1–23 (1973).

17. Riahi, K. *et al.* The Shared Socioeconomic Pathways and their energy, land use, and greenhouse gas emissions implications: An overview. *Glob. Environ. Chang.* **42**, 153–168 (2017).

18. Meinshausen, M. *et al.* The shared socio-economic pathway (SSP) greenhouse gas concentrations and their extensions to 2500. *Geosci. Model Dev.* **13**, 3571–3605 (2020).

19. Scheffers, B. R. *et al.* The broad footprint of climate change from genes to biomes to people. *Science (80-.).* **354**, (2016).

20. Pinsky, M. L., Eikeset, A. M., McCauley, D. J., Payne, J. L. & Sunday, J. M. Greater vulnerability to warming of marine versus terrestrial ectotherms. *Nature* (2019) doi:10.1038/s41586-019-1132-4.

21. Stuart-Smith, R. D., Edgar, G. J., Barrett, N. S., Kininmonth, S. J. & Bates, A. E. Thermal biases and vulnerability to warming in the world's marine fauna. *Nature* **528**, 88+ (2015).

22. Sunday, J. M., Bates, A. E. & Dulvy, N. K. Thermal tolerance and the global redistribution of animals. *Nat. Clim. Chang.* **2**, 686–690 (2012).

23. Laidre, K. L. *et al.* Quantifying the sensitivity of Arctic marine mammals to climate-induced habitat change. *Ecol. Appl.* **18**, S97-125 (2008).

24. Rosset, V. & Oertli, B. Freshwater biodiversity under climate warming pressure: Identifying the winners and losers in temperate standing waterbodies. *Biol. Conserv.* **144**, (2011).

25. Peters, R. L. The Greenhouse Effect and Nature Reserves. *Biosciences* **35**, 707–717 (1985).

26. Garcia, R. A. *et al.* Matching species traits to projected threats and opportunities from climate change. *J. Biogeogr.* **41**, 724–735 (2014).

27. IUCN. *IUCN Red List Categories and Criteria: Version 3.1*. (IUCN, 2012).

28. Worm, B. *et al.* Impacts of biodiversity loss on ocean ecosystem services. *Science (80-.).* **314**, 787–90 (2006).

29. Worm, B., Lotze, H. K., Hillebrand, H. & Sommer, U. Consumer versus resource control of species diversity and ecosystem functioning. *Nature* **417**, 848–851 (2002).

30. Worm, B. & Duffy, J. E. Biodiversity, productivity, and stability in real food webs. *Trends Ecol. Evol.* **18**, 628–632 (2003).

31. Halpern, B. S. *et al.* A global map of human impact on marine ecosystems. *Science (80-.).* **319**, 948–952 (2008).

32. Halpern, B. S. *et al.* An index to assess the health and benefits of the global ocean. *Nature* **488**, 615–620 (2012).

33. Halpern, B. S. *et al.* Spatial and temporal changes in cumulative human impacts on the world's ocean. *Nat. Commun.* **6**, 1–7 (2015).

34. Ottersen, G., Hjermann, D. O. & Stenseth, N. C. Changes in spawning stock structure strengthen the link between climate and recruitment in a heavily fished cod (Gadus morhua) stock. *Fish. Oceanogr.* **15**, 230–243 (2006).

35. Le Bris, A. *et al.* Climate vulnerability and resilience in the most valuable North American fishery. *Proc. Natl. Acad. Sci. U. S. A.* **115**, 1831–1836 (2018).

36. Henson, S. A. *et al.* Rapid emergence of climate change in environmental drivers of marine ecosystems. *Nat. Commun.* **8**, 1–9 (2017).

37. Bates, A. E. *et al.* Climate resilience in marine protected areas and the 'Protection Paradox'. *Biol. Conserv.* **236**, 305–314 (2019).

38. Trisos, C. H., Merow, C. & Pigot, A. L. The projected timing of abrupt ecological disruption from climate change. *Nature* **580**, 1–6 (2020).

39. Xu, C., Kohler, T. A., Lenton, T. M., Svenning, J.-C. & Scheffer, M. Future of the human climate niche. *Proc. Natl. Acad. Sci.* **117**, 11350–11355 (2020).

40. Davies, T. E., Maxwell, S. M., Kaschner, K., Garilao, C. & Ban, N. C. Large marine protected areas represent biodiversity now and under climate change. *Sci. Rep.* **7**, 1–7 (2017).

41. MacKenzie, B. R. *et al.* A cascade of warming impacts brings bluefin tuna to Greenland waters. *Glob. Chang.*

Biol. **20**, 2484–2491 (2014).

42. Shackell, N. L., Ricard, D. & Stortini, C. Thermal habitat index of many Northwest Atlantic temperate species stays neutral under warming projected for 2030 but changes radically by 2060. *PLoS One* **9**, (2014).

43. Boyce, D. G., Frank, K. T., Worm, B. & Leggett, W. C. Spatial patterns and predictors of trophic control across marine ecosystems. *Ecol. Lett.* **18**, 1001–1011 (2015).

44. Boyce, D. G., Frank, K. T. & Leggett, W. C. From mice to elephants: overturning the 'one size fits all' paradigm in marine plankton food chains. *Ecol. Lett.* **18**, 504–515 (2015).

45. Frank, K. T., Petrie, B., Shackell, N. L. & Choi, J. S. Reconciling differences in trophic control in mid-latitude marine ecosystems. *Ecol. Lett.* **9**, 1096–1105 (2006).

46. Frank, K. T., Petrie, B. & Shackell, N. L. The ups and downs of trophic control in continental shelf ecosystems. *Trends Ecol. Evol.* **22**, 236–242 (2007).

47. Loarie, S. R. *et al.* The velocity of climate change. *Nature* **462**, 1052–1056 (2009).

48. Burrows, M. T. *et al.* The Pace of Shifting Climate in Marine and Terrestrial Ecosystems. *Science (80-.).* **334**, 652–655 (2011).

49. Mora, C. *et al.* The projected timing of climate departure from recent variability. *Nature* **502**, 183+ (2013).

50. Poloczanska, E. S. *et al.* Responses of Marine Organisms to Climate Change across Oceans. *Front. Mar. Sci.* **3**, 62 (2016).

51. Boyce, D. G., Lotze, H. K., Tittensor, D. P., Carozza, D. A. & Worm, B. Future ocean biomass losses may widen socioeconomic equity gaps. *Nat. Commun.* (2020).

52. Boyce, D. G., Lewis, M. L. & Worm, B. Global phytoplankton decline over the past century. *Nature* **466**, 591–596 (2010).

53. Burek, K. A., Gulland, F. M. D. & O'Hara, T. M. Effects of climate change on Arctic marine mammal health. *Ecol. Appl.* **18**, S126–S134 (2008).

54. Staude, I. R., Navarro, L. M. & Pereira, H. M. Range size predicts the risk of local extinction from habitat loss. *Glob. Ecol. Biogeogr.* **29**, 16–25 (2020).

55. Moore, S. E. & Huntington, H. P. Arctic marine mammals and climate change: impacts and resilience. *Ecol. Appl.* **18**, S157–S165 (2008).

56. Kaschner, K., Watson, R., Trites, A. & Pauly, D. Mapping world-wide distributions of marine mammal species using a relative environmental suitability (RES) model. *Mar. Ecol. Prog. Ser.* **316**, 285–310 (2006).

57. Gonzalez-Suarez, M., Gomez, A. & Revilla, E. Which intrinsic traits predict vulnerability to extinction depends on the actual threatening processes. *Ecosphere* **4**, 1–16 (2013).

58. Rogan, J. E. & Lacher, T. E. Impacts of Habitat Loss and Fragmentation on Terrestrial Biodiversity. in *Reference Module in Earth Systems and Environmental Sciences* (Elsevier, 2018). doi:10.1016/B978-0-12-409548-9.10913-3.

59. Warren, M. S. *et al.* Rapid responses of British butterflies to opposing forces of climate and habitat change. *Nature* **414**, 65–69 (2001).

60. Chessman, B. C. Identifying species at risk from climate change: Traits predict the drought vulnerability of freshwater fishes. *Biol. Conserv.* **160**, 40–49 (2013).

61. Davidson, A. D. D. *et al.* Drivers and hotspots of extinction risk in marine mammals. *Proc. Natl. Acad. Sci.* **109**, 3395–3400 (2012).

62. Cheung, W. W. L., Pauly, D. & Sarmiento, J. L. How to make progress in projecting climate change impacts. *ICES J. Mar. Sci.* **70**, 1069–1074 (2013).

63. Fenchel, T. Intrinsic rate of natural increase: The relationship with body size. *Oecologia* **14**, 317–326 (1974).

64. Healy, K. *et al.* Ecology and mode-of-life explain lifespan variation in birds and mammals. *Proc. R. Soc. B Biol. Sci.* **281**, 20140298 (2014).

65. Carilli, J., Donner, S. D. & Hartmann, A. C. Historical Temperature Variability Affects Coral Response to Heat Stress. *PLoS One* **7**, e34418 (2012).

66. Guest, J. R. *et al.* Contrasting Patterns of Coral Bleaching Susceptibility in 2010 Suggest an Adaptive Response to Thermal Stress. *PLoS One* **7**, e33353 (2012).

67. Donner, S. D. & Carilli, J. Resilience of Central Pacific reefs subject to frequent heat stress and human disturbance. *Sci. Rep.* **9**, 3484 (2019).

68. Rehm, E. M., Olivas, P., Stroud, J. & Feeley, K. J. Losing your edge: climate change and the conservation value of range-edge populations. *Ecol. Evol.* **5**, 4315–4326 (2015).

69. IUCN. The IUCN Red List of Threatened Species. *Version 2021-1* https://www.iucnredlist.org (2021).

70. Stuart-Smith, R. D., Edgar, G. J., Barrett, N. S., Kininmonth, S. J. & Bates, A. E. Thermal biases and vulnerability to warming in the world € s marine fauna. *Nature* **528**, 88–92 (2015).

71. Pearson, R. G. *et al.* Life history and spatial traits predict extinction risk due to climate change. *Nat. Clim. Chang.* **4**, 217–221 (2014).

72. Gallagher, R. V., Allen, S. & Wright, I. J. Safety margins and adaptive capacity of vegetation to climate change. *Sci. Rep.* **9**, 8241 (2019).

73. Butt, N. *et al.* A trait-based framework for assessing the vulnerability of marine species to human impacts. *Ecosphere* **13**, (2022).

74. Ficetola, G. F. & Denoel, M. Ecological thresholds: an assessment of methods to identify abrupt changes in species-habitat relationships. *Ecography (Cop.).* **32**, 1075–1084 (2009).

75. Cheung, W. W. L., Watson, R., Morato, T., Pitcher, T. J. & Pauly, D. Intrinsic vulnerability in the global fish catch. *Mar. Ecol. Prog. Ser.* **333**, 1–12 (2007).

76. Chase, J. M., Blowes, S. A., Knight, T. M., Gerstner, K. & May, F. Ecosystem decay exacerbates biodiversity loss with habitat loss. *Nature* **584**, 238–243 (2020).

77. Brown, J. H. & Kodric-Brown, A. Turnover Rates in Insular Biogeography: Effect of Immigration on Extinction. *Ecology* **58**, 445–449 (1977).

78. Lehtinen, R. M., Galatowitsch, S. M. & Tester, J. R. Consequences of habitat loss and fragmentation for wetland amphibian assemblages. *Wetlands* **19**, 1–12 (1999).

79. Fahrig, L. Effect of habitat fragmentation on the extinction threshold: A synthesis. *Ecol. Appl.* **12**, 346–353 (2002).

80. Rueda, M. *et al.* Does fragmentation increase extinction thresholds? A European-wide test with seven forest birds. *Glob. Ecol. Biogeogr.* **22**, 1282–1292 (2013).

81. Palmeirim, A. F., Santos-Filho, M. & Peres, C. A. Marked decline in forest-dependent small mammals following habitat loss and fragmentation in an Amazonian deforestation frontier. *PLoS One* **15**, e0230209 (2020).

82. Crooks, K. R. *et al.* Quantification of habitat fragmentation reveals extinction risk in terrestrial mammals. *Proc. Natl. Acad. Sci.* **114**, 7635–7640 (2017).

83. Cheung, W. W. L. & Oyinlola, M. A. Vulnerability of flatfish and their fisheries to climate change. *J. Sea Res.* **140**, 1–10 (2018).

84. Blueweiss, L. *et al.* Relationships between body size and some life history parameters. *Oecologia* **37**, 257–272 (1978).

85. Ripple, W. J. *et al.* Extinction risk is most acute for the world's largest and smallest vertebrates. *Proc. Natl. Acad. Sci.* **114**, 10678–10683 (2017).

86. Nadeau, C. P., Urban, M. C. & Bridle, J. R. Climates past, present, and yet-to-come shape climate change vulnerabilities. *Trends Ecol. Evol.* **32**, 786–800 (2017).

87. Cole, L. E. S., Bhagwat, S. A. & Willis, K. J. Recovery and resilience of tropical forests after disturbance. *Nat. Commun.* **5**, 3906 (2014).

88. Mora, C., Danovaro, R. & Loreau, M. Alternative hypotheses to explain why biodiversity-ecosystem functioning relationships are concave-up in some natural ecosystems but concave-down in manipulative experiments. *Sci. Rep.* **4**, 5427 (2014).

89. Xu, Y. *et al.* The exposure, sensitivity and vulnerability of natural vegetation in China to climate thermal variability (1901–2013): An indicator-based approach. *Ecol. Indic.* **63**, 258–272 (2016).

90. Li, D., Wu, S., Liu, L., Zhang, Y. & Li, S. Vulnerability of the global terrestrial ecosystems to climate change. *Glob. Chang. Biol.* **24**, 4095–4106 (2018).

91. Martin, T. G. & Watson, J. E. M. Intact ecosystems provide best defence against climate change. *Nat. Clim. Chang.* **6**, 122–124 (2016).

92. Bruno, J. F. *et al.* Climate change threatens the world's marine protected areas. *Nat. Clim. Chang.* **8**, 499–503 (2018).

93. Pinsky, M. L., Worm, B., Fogarty, M. J., Sarmiento, J. L. & Levin, S. A. Marine Taxa Track Local Climate Velocities. *Science (80-.).* **341**, 1239–1242 (2013).

94. Ochoa-Quintero, J. M., Gardner, T. A., Rosa, I., de Barros Ferraz, S. F. & Sutherland, W. J. Thresholds of species loss in Amazonian deforestation frontier landscapes. *Conserv. Biol.* **29**, 440–451 (2015).

95. Stortini, C. H. C. H., Shackell, N. L. N. L., Tyedmers, P. & Beazley, K. Assessing marine species vulnerability to projected warming on the Scotian Shelf, Canada. *ICES J. Mar. Sci.* **72**, 1713–1743 (2015).

96. Greenan, B. J. W. *et al.* Climate Change Vulnerability of American Lobster Fishing Communities in Atlantic Canada. *Front. Mar. Sci.* **6**, 1–18 (2019).

97. McHenry, J., Welch, H., Lester, S. E. & Saba, V. Projecting marine species range shifts from only temperature can mask climate vulnerability. *Glob. Chang. Biol.* **25**, 4208–4221 (2019).

98. Boyce, D. G., Schleit, K. & Fuller, S. *Incorporating climate change into fisheries management in Atlantic Canada and the Eastern Arctic*. (2021).

99. Kaschner, K. *et al.* Aquamaps: Predicted range maps for aquatic species. (2019).

100. *FishBase 2000: concepts, design and data sources*. (Los Banos, 2000).

101. Palomares, M. L. D. & Pauly, D. SeaLifeBase. *World Wide Web Electron. Publ. www.sealifebase.org, version (11/2014).* (2014).

102. Horton, T. *et al.* World Register of Marine Species (WoRMS). (2020).

103. *Gebco gridded global bathymetry data*. (British Oceanographic Data Centre, 2009).

104. Reynolds, R. W. *et al.* Daily high-resolution-blended analyses for sea surface temperature. *J. Clim.* **20**, 5473–5496 (2007).

105. Eyring, V. *et al.* Overview of the Coupled Model Intercomparison Project Phase 6 (CMIP6) experimental design and organization. *Geosci. Model Dev.* **9**, 1937–1958 (2016).

106. Guiry, M. D. & Guiry, G. M. AlgaeBase. World-wide electronic publication. *National University of Ireland, Galway* (2021).

107. Ready, J. *et al.* Predicting the distributions of marine organisms at the global scale. *Ecol. Modell.* **221**, 467–478 (2010).

108. Jones, M. C., Dye, S. R., Pinnegar, J. K., Warren, R. & Cheung, W. W. L. Modelling commercial fish distributions: Prediction and assessment using different approaches. *Ecol. Modell.* **225**, 133–145 (2012).

109. Bennett, J. M. *et al.* GlobTherm, a global database on thermal tolerances for aquatic and terrestrial organisms. *Sci. Data* **5**, 180022 (2018).

110. Wu, T. *et al.* The Beijing Climate Center Climate System Model (BCC-CSM): the main progress from CMIP5 to CMIP6. *Geosci. Model Dev.* **12**, 1573–1600 (2019).

111. Volodin, E. M. *et al.* Simulation of the modern climate using the INM-CM48 climate model. *Russ. J. Numer. Anal. Math. Model.* **33**, 367–374 (2018).

112. Tatebe, H. *et al.* Description and basic evaluation of simulated mean state, internal variability, and climate sensitivity in MIROC6. *Geosci. Model Dev.* **12**, 2727–2765 (2019).

113. Yukimoto, S. *et al.* The Meteorological Research Institute Earth System Model Version 2.0, MRI-ESM2.0: Description and Basic Evaluation of the Physical Component. *J. Meteorol. Soc. Japan. Ser. II* **97**, 931–965 (2019).

114. Bi, D. *et al.* Configuration and spin-up of ACCESS-CM2, the new generation Australian Community Climate and Earth System Simulator Coupled Model. *J. South. Hemisph. Earth Syst. Sci.* **70**, 225 (2020).

115. Rong, X.-Y. *et al.* Introduction of CAMS-CSM model and its participation in CMIP6. *Clim. Chang. Res.* **5**, 540–44 (2019).

116. Cherchi, A. *et al.* Global mean climate and main patterns of variability in the CMCC-CM2 coupled model. *J. Adv. Model. Earth Syst.* 2018MS001369 (2018) doi:10.1029/2018MS001369.

117. He, B. *et al.* CAS FGOALS-f3-L Model Datasets for CMIP6 Historical Atmospheric Model Intercomparison Project Simulation. *Adv. Atmos. Sci.* **36**, 771–778 (2019).

118. Bao, Y., Song, Z. & Qiao, F. FIO-ESM Version 2.0: Model Description and Evaluation. *J. Geophys. Res. Ocean.* **125**, (2020).

119. Lee, J. *et al.* Evaluation of the Korea Meteorological Administration Advanced Community Earth-System model (K-ACE). *Asia-Pacific J. Atmos. Sci.* **56**, 381–395 (2020).

120. Pak, G. *et al.* Korea Institute of Ocean Science and Technology Earth System Model and Its Simulation Characteristics. *Ocean Sci. J.* **56**, 18–45 (2021).

121. Cao, J. *et al.* The NUIST Earth System Model (NESM) version 3: description and preliminary evaluation. *Geosci. Model Dev.* **11**, 2975–2993 (2018).

122. Samhouri, J. F. *et al.* Sea sick? Setting targets to assess ocean health and ecosystem services. *Ecosphere* **3**, art41 (2012).

123. Rao, T. R. A Curve for all reasons. *Resonance* **5**, 85–90 (2000).

124. Ves, A. R. I. *et al.* Estimating community stability and ecological interactions from time-series data. *Ecol. Monogr.* **73**, 301–330 (2003).

125. Le Bris, A., Pershing, A. J., Hernandez, C. M., Mills, K. E. & Sherwood, G. D. Modelling the effects of variation in reproductive traits on fish population resilience. *ICES J. Mar. Sci.* **72**, 2590–2599 (2015).

126. Froese, R. & Pauly, D. FishBase: World Wide Web electronic publication. www.fishbase.org, version (12/2004). (2004).

127. Frank, K. T. T., Petrie, B., Choi, J. S. S. & Leggett, W. C. C. Trophic cascades in a formerly cod-dominated ecosystem. *Science (80-.).* **308**, 1621–1623 (2005).

128. Frank, K. T., Petrie, B., Fisher, J. A. D. & Leggett, W. C. Transient dynamics of an altered large marine ecosystem. *Nature* **477**, 86–89 (2011).

129. Estes, J. a., Tinker, M. T., Williams, T. M. & Doak, D. F. Killer Whale Predation on Sea Otters Linking Oceanic and Nearshore Ecosystems. *Science (80-.).* **282**, 473–476 (1998).

130. Garciá Molinos, J. *et al.* Climate velocity and the future global redistribution of marine biodiversity. *Nat. Clim. Chang.* **6**, 83–88 (2016).

131. Brito-Morales, I. *et al.* Climate Velocity Can Inform Conservation in a Warming World Simple Climate Metrics Could Help Conservation in a Changing Climate. *Trends Ecol. Evol.* **33**, 1–17 (2018).

132. García Molinos, J., Schoeman, D. S., Brown, C. J. & Burrows, M. T. VoCC: An R package for calculating the velocity of climate change and related climatic metrics. *Methods Ecol. Evol.* **10**, 2195–2202 (2019).

133. McGarigal, K. & Cushman, S. A. FRAGSTATS v4: Spatial Pattern Analysis Program for Categorical and Continuous Maps. Computer software program produced by the authors at the University of Massachusetts, Amherst. (2012).

134. Hesselbarth, M. H. K., Sciaini, M., With, K. A., Wiegand, K. & Nowosad, J. Landscapemetrics: an open-source R tool to calculate landscape metrics. *Ecography (Cop.).* **42**, 1648–57 (2019).

135. Mora, C. *et al.* Suitable Days for Plant Growth Disappear under Projected Climate Change: Potential Human and Biotic Vulnerability. *PLoS Biol.* **13**, e1002167 (2015).

136. Mora, C. *et al.* Biotic and human vulnerability to projected changes in ocean biogeochemistry over the 21st

century. *PLoS Biol.* **11**, 1–14 (2013).

137. Lotze, H. K. *et al.* Ensemble projections of global ocean animal biomass with climate change. *Proc. Natl. Acad. Sci.* 1–6 (2019) doi:doi.org/10.1073/pnas.1900194116.

138. Eyring, V. *et al.* Taking climate model evaluation to the next level. *Nat. Clim. Chang.* **9**, 102–110 (2019).

139. Thurman, L. L. *et al.* Persist in place or shift in space? Evaluating the adaptive capacity of species to climate change. *Front. Ecol. Environ.* **18**, 520–528 (2020).

140. Hillebrand, H. *et al.* Thresholds for ecological responses to global change do not emerge from empirical data. *Nat. Ecol. Evol.* **4**, 1502–1509 (2020).

141. van der Hoek, Y., Zuckerberg, B. & Manne, L. L. Application of habitat thresholds in conservation: Considerations, limitations, and future directions. *Glob. Ecol. Conserv.* **3**, 736–743 (2015).

142. Shennan-Farpón, Y., Visconti, P. & Norris, K. Detecting ecological thresholds for biodiversity in tropical forests: Knowledge gaps and future directions. *Biotropica* btp.12999 (2021) doi:10.1111/btp.12999.

143. Arroyo-Rodríguez, V. *et al.* Designing optimal human-modified landscapes for forest biodiversity conservation. *Ecol. Lett.* **23**, 1404–1420 (2020).

144. Rockström, J. *et al.* A safe operating space for humanity. *Nature* **461**, 472–475 (2009).

145. IPCC. *Climate Change 2021: The Physical Science Basis. Contribution of Working Group I to the Sixth Assessment Report of the Intergovernmental Panel on Climate Change*. (Cambridge University Press. In press., 2021).

146. IPCC. *Climate Change 2001: Impacts, Adaptation, and Vulnerability. Contribution of Working Group II to the Third Assessment Report of the Intergovernmental Panel on Climate Change (IPCC)*. (Cambridge University Press, 2001).

147. Zommers, Z. *et al.* Burning embers: towards more transparent and robust climate-change risk assessments. *Nat. Rev. Earth Environ.* **1**, 516–529 (2020).

148. Leemans, R. & Vellinga, P. The scientific motivation of the internationally agreed 'well below 2 degrees C' climate protection target: a historical perspective. *Curr. Opin. Environ. Sustain.* **26**–**27**, 134–142 (2017).

149. Fischlin, A. Do We Have Sufficient Safety Margins in Climate Policy? *GAIA-ECOLOGICAL Perspect. Sci. Soc.* **18**, 193–199 (2009).

150. Garner, G., Reed, P. & Keller, K. Climate risk management requires explicit representation of societal trade-offs. *Clim. Change* **134**, 713–723 (2016).

151. Oppenheimer, M., Little, C. M. & Cooke, R. M. Expert judgement and uncertainty quantification for climate change. *Nat. Clim. Chang.* **6**, 445–451 (2016).

152. Budescu, D. V, Por, H. H. & Broomell, S. B. Effective communication of uncertainty in the IPCC reports. *Clim. Change* **113**, 181–200 (2012).

153. Swart, R., Bernstein, L., Ha-Duong, M. & Petersen, A. Agreeing to disagree: uncertainty management in assessing climate change, impacts and responses by the IPCC. *Clim. Change* **92**, 1–29 (2009).

154. Gattuso, J.-P. J.-P. P. *et al.* Contrasting futures for ocean and society from different anthropogenic CO2 emissions scenarios. *Science (80-.).* **349**, aac4722-1-aac4722-10 (2015).

155. Yin, D., Leroux, S. J. & He, F. Methods and models for identifying thresholds of habitat loss. *Ecography (Cop.).* **40**, 131–143 (2017).

156. Swift, T. L. & Hannon, S. J. Critical thresholds associated with habitat loss: a review of the concepts, evidence, and applications. *Biol. Rev.* **85**, 35–53 (2010).

157. Homan, R. N., Windmiller, B. S. & Reed, J. M. Critical thresholds associated with habitat loss for two vernal pool-breeding amphibians. *Ecol. Appl.* **14**, 1547–1553 (2004).

158. Lange, R., Durka, W., Holzhauer, S. I. J., Wolters, V. & Diekotter, T. Differential threshold effects of habitat fragmentation on gene flow in two widespread species of bush crickets. *Mol. Ecol.* **19**, 4936–4948 (2010).

159. Oliver, T. H. How much biodiversity loss is too much? *Science (80-.).* **353**, 220–221 (2016).

160. Brose, U. & Hillebrand, H. Biodiversity and ecosystem functioning in dynamic landscapes. *Philos. Trans. R. Soc. B Biol. Sci.* **371**, 20150267 (2016).

161. Newbold, T. *et al.* Has land use pushed terrestrial biodiversity beyond the planetary boundary? A global assessment. *Science (80-.).* **353**, 288–291 (2016).

162. Scholes, R. J. & Biggs, R. A biodiversity intactness index. *Nature* **434**, 45–49 (2005).

163. Hooper, D. U. *et al.* A global synthesis reveals biodiversity loss as a major driver of ecosystem change. *Nature* **486**, 105–8 (2012).

164. FRYE, R. Variability and management of large marine ecosystems - Sherman, K, Alexander, LM. *Nat. Resour. J.* **26**, 653–654 (1986).

165. Longhurst, A. *Ecological geography of the sea*. (Elsevier Inc., 2007).

166. Boyce, D. G., Petrie, B., Frank, K. T., Worm, B. & Leggett, W. C. Environmental structuring of marine plankton phenology. *Nat. Ecol. Evol.* 0–1 (2017) doi:10.1038/s41559-017-0287-3.

167. Mann, K. H. & Lazier, J. R. N. *Dynamics of marine ecosystems*. (Blackwell, 1991).

168. Gattuso, J. P. *et al.* Contrasting futures for ocean and society from different anthropogenic CO2 emissions scenarios. *Science (80-.).* **349**, (2015).

169. Rompre, G., Boucher, Y., Belanger, L., Cote, S. & Robinson, W. D. Conserving biodiversity in managed forest landscapes: The use of critical thresholds for habitat. *For. Chron.* **86**, 589–596 (2010).

170. Liao, J. *et al.* Modelling plant population size and extinction thresholds from habitat loss and habitat fragmentation: Effects of neighbouring competition and dispersal strategy. *Ecol. Modell.* **268**, 9–17 (2013).

171. Parker, M. & Mac Nally, R. Habitat loss and the habitat fragmentation threshold: an experimental evaluation of impacts on richness and total abundances using grassland invertebrates. *Biol. Conserv.* **105**, 217–229 (2002).

172. Andren, H. Effects of habitat fragmentation on birds and mammals in landscapes with different proportions of suitable habitat: a review. *OIKOS* **71**, 355–366 (1994).

173. Hill, M. F. & Caswell, H. Habitat fragmentation and extinction thresholds on fractal landscapes. *Ecol. Lett.* **2**, 121–127 (1999).

174. Garcia, H. E. *et al.* World Ocean Atlas 2018: Product Documentation. in (ed. Mishonov, A.) (2019).

175. Ellington, E. H. *et al.* Using multiple imputation to estimate missing data in meta-regression. *Methods Ecol. Evol.* **6**, 153–163 (2015).

176. Zhao, Q. *et al.* Where Marine Protected Areas would best represent 30% of ocean biodiversity. *Biol. Conserv.* **244**, 108536 (2020).

177. Brito-Morales, I. *et al.* Climate velocity reveals increasing exposure of deep-ocean biodiversity to future warming. *Nat. Clim. Chang.* **10**, 576–581 (2020).

178. Venegas-Li, R. *et al.* Global assessment of marine biodiversity potentially threatened by offshore hydrocarbon activities. *Glob. Chang. Biol.* **25**, 2009–2020 (2019).

179. Fox, J. & Monette, G. Generalized Collinearity Diagnostics. *J. Am. Stat. Assoc.* **87**, 178–83 (1992).

180. Tittensor, D. P. *et al.* Global patterns and predictors of marine biodiversity across taxa. *Nature* **466**, 1098–1101 (2010).